Materials & Design 210 (2021) 110100

Contents lists available at ScienceDirect

Materials & Design

journal homepage: www.elsevier.com/locate/matdes

Waste not, want not: The use of leather waste in flame retarded EVA

A. Battig [a], G. Sanchez-Olivares [b], D. Rockel [a], M. Maldonado-Santoyo [b], B. Schartel [a,*]

[a] Bundesanstalt für Materialforschung und -prüfung (BAM), Unter den Eichen 87, 12205 Berlin, Germany
[b] CIATEC A.C, Omega 201, Colonia Industrial Delta, Léon, Gto 37545, Mexico

HIGHLIGHTS

- Wastes from leather production are upcycled as sustainable fillers for polymer composites.
- Leather waste is an adjuvant and synergist to phosphorus flame retardants that decrease the fire load of poly(ethylene–vinyl acetate).
- The main modes of action, which include enhanced residue formation and stabilization, are explored and characterized multi-methodically.
- The combination of flame retardant and filler exhibit better fire performance than equal loadings of only flame retardant.
- The chemical mechanisms of flame retardancy are elucidated to explain the fire phenomena.

GRAPHICAL ABSTRACT

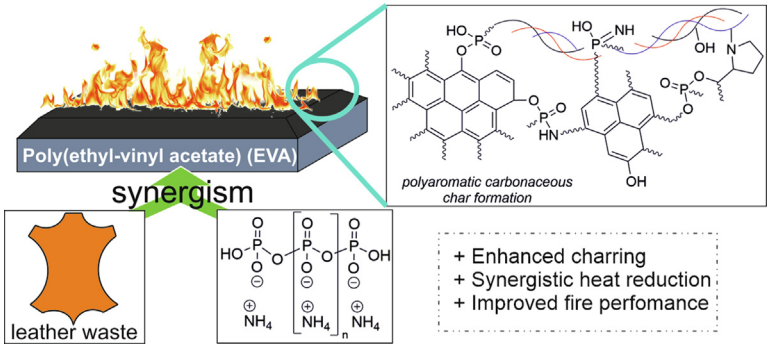

ARTICLE INFO

Article history:
Received 11 June 2021
Revised 13 August 2021
Accepted 6 September 2021
Available online 15 September 2021

Keywords:
Leather waste
Tannery industry
EVA
Fire protection
Flame retardancy
Charring

ABSTRACT

Leather is among the most ancient, widely used materials worldwide. Industrial-scale leather production produces large quantities of organic waste attained during shaving and buffing steps during processing. In this study, leather wastes (LW) are used as fillers in flame retarded polymer composites. LW is investigated as a multifunctional bio-filler that enhances the fire performance of flame retarded poly(ethylene–vinyl acetate) (EVA) containing phosphorus flame retardants (P-FRs) ammonium polyphosphate (APP) or a melamine-encapsulated APP (eAPP). Using LW from tanneries as adjuvants to enhance P-FRs in EVA reduces industrial wastes that otherwise require costly waste management solutions. Materials are characterized multi-methodically via mechanical tests, electron microscopy, rheology, thermogravimetric analysis, evolved gas analysis, and condensed phase FTIR, also reaction-to-small-flames and cone calorimeter tests. EVA containing 10 wt-% LW and 20 wt-% P-FRs achieve 20% reductions in fire loads versus EVA, and up to 10% reduction in effective heats of combustion versus EVA with equal (30 wt-%) P-FR loadings. Enhanced char stabilization of EVA composites with LW and P-FRs lowered peaks of heat release rates up to 53% compared to EVA, and up to 40% compared to equal P-FRs loadings. Synergisms between LW and P-FRs in EVA are quantified. A chemical decomposition mechanism is proposed.

1. Introduction

The leather industry is one of the oldest manufacturing sectors; the raw materials used in leather industry are derived from live-

* Corresponding author.
E-mail addresses: gsanchez@ciatec.mx (G. Sanchez-Olivares), bernhard.schartel@bam.de (B. Schartel).

https://doi.org/10.1016/j.matdes.2021.110100
0264-1275/

stock or the animal farming industry. The production of leather goods requires the raw material to be put through different stages and includes several steps: Tanning is the first stage, and once leather is tanned (wet leather), it is thinned such that the thickness is adjusted according to the end use of leather (e.g. footwear, upholstery, clothing, etc.). This step is carried out using a leather shaving machine which cuts off leather fibers from the flesh side. Afterwards, the leather is re-tanned, fat-liquored, and dyed, and finally, it is finishing by oiling, brushing, impregnation, polishing, tumbling among others, depending on the required quality [1]. During the wet-leather shaving step, leather fibers are derived as solid wastes, which are mainly treated as industrial landfill [2]. Mexico is among the top 10 largest leather producing countries, and according to the International Council of Tanners, the annual production of the Mexican leather industry is estimated at 642 million square feet [3]. Therefore, in local areas where this industry is the main economic activity, effluents and solid wastes are disposal problems that require special attention, especially because of the environmental concerns from landfill disposal.

The idea of valorizing, repurposing, or "up-cycling" wastes from any manufacturing process is a key concept in the promotion of circular economies, and several studies have investigated the use of natural fibers in biocomposites [4,5], as well as their flame-retardant properties in combination with phosphorus flame retardants [6,7]. Aimed at proposing approaches that improve the sustainability of polymer materials while contributing to the reduction of local industrial solid disposals, leather wastes (LW) from shaving and buffing steps have been purposed as fillers in the manufacturing of polymer composites in several studies. Vulcanized natural rubber mixed with buffed, stripped, and shaved LW along with carbon black were processed by thermal compression to obtain an antistatic flooring; composites with added LW presented increased electrical conductivity and were able to withstand exposure to sanitizing agents. This improvement was ascribed to the good load distribution in the composite due to reactivity of carbon black and LW [8]. In another study, varying LW contents were incorporated into polylactic acid (PLA) to obtain eco-biocomposites: The materials presented improved tensile properties and reduced crystallinity with increasing LW content, which was explained by the good dispersion and efficient stress-transfer of LW at relatively low content (<10 wt-%). When LW was added at 20 or 30 wt-% loadings, the morphology of tensile fracture surfaces of the composites revealed fiber bundle pull-out, a weak PLA-fiber interface, and fracture failures due to poorly dispersed LW; this resulted in overall low tensile properties for the biocomposites [9]. LW as a reinforcement to other biodegradable polymers such as polycaprolactone (PCL) was previously studied [10]: the addition of up to 20 wt-% LW to PCL presented similar stress–strain behavior of the composites with respect to the polymer matrix. The use of 30–40 wt-% LW content produced brittle materials, the Young's modulus increased, and elongation at break was highly affected; the mechanical behavior of high LW-content PCL composites was attributed to the presence of LW aggregates in the polymer matrix, which produced stress points and caused an inefficient wetting of LW. The effect of LW on mechanical properties and thermal stability in thermoplastic polymer acrylonitrile–butadienestyrene (ABS) composites was investigated as well. Several physical and mechanical properties were evaluated, e.g., tensile and flexural properties, Izod and Charpy impact resistance, abrasion weight loss, Rockwell hardness, and density. It was found that mechanical strength was reduced as LW load increased; the results were attributed to poor interfacial bonding due to opposite polarities between the ABS resin and LW. In thermal stability investigations, ABS-LW composites presented better thermal stability than the pure polymer matrix with respect to residue production at 500–600 °C [11].

Thus, research has shown that LW is a multifunctional bio-based filler for many polymer matrices, however, its flame-retardancy potential has not been analyzed in-depth. This work examines whether LW can enhance the material and flame-retardant properties of thermoplastic poly(ethylene–vinyl acetate) (EVA) containing phosphorus flame retardants (P-FRs). EVA is a copolymer of ethylene and vinyl acetate that is a type of thermoplastic elastomer material; its properties are determined by the amount of vinyl acetate. Its main commercial uses are hot melt adhesives, or as a thermoplastic foam rubber, and EVA is also used in cables as a coating material. Due to its inherent flammability, flame retardants are necessary, and some studies have shown that ammonium polyphosphate (APP) as well as melamine microencapsulated APP (eAPP) are effective inorganic phosphorus flame retardants in EVA composites, showing improved electrical insulation, material properties, and fire performance [12]. Inorganic P-FR additives are an efficient and environmentally friendly alternative to halogen-based additives for many polymer matrices. The effect of P-FR additives has been also investigated in combination with natural fibers, e.g., APP with wood flakes and corn shell in different polymer matrices [13,14]. The combination of APP and natural fibers showed a significant improvement on flame retardancy of polymer composites via charring effects. These results demonstrated a viable route to obtain flame retarded natural fiber reinforced composites [15]. The synergistic effect of APP between keratin fibers, derived from tannery waste, and coconut fibers on the flame-retardant behavior of thermoplastic starch biocomposites was exposed and explained in detail [16]. Moreover, the idea of utilizing waste products from industries as flame-retardant enhancing fillers was further explored in a study where agave and henequen fibers were compounded with aluminum diethyl phosphinate (AlPi) and a special silicone synergist in thermoplastic starch composites; the results highlighted the ability of these fibers to enhance the flame retardancy potential of AlPi and provide gas and condensed phase modes of action [17].

This study aims at investigating the flame retardancy potential of LW as an adjuvant to P-FRs in EVA composites. Research on the flammability and burning behavior of LW, attained from the shaving step in the production of leather, as a filler in polymer composites is still limited. In this work, the potential of wet-white leather wastes as adjuvants in flame retarded EVA polymer composites are assessed and the resulting physical–mechanical properties of the obtained materials are investigated. The composites' fire behavior is assessed with the aim of understanding the chemical flame retardancy mechanisms at work in fire scenarios. The investigation aims at evaluating how leather waste from industries harbor the potential to enhance the fire properties of APP or melamine-encapsulated APP in EVA polymers.

2. Materials and methods

The main structural protein in leather waste (LW) is collagen; its unique chemical structure has been extensively analysed [18,19]. Fig. 1 displays the chemical structure of the amino acids found in collagen, the respective three-letter codes [20]; the amino acids are listed in order of their relative abundance [21]. The prevalence of sequences Gly-Pro-Xaa or Gyl–Hyp–Xaa result in the formation of the helical tropocollagen structure. Proline and hydroxyproline contain cyclic pyrrolidine-like structures. Resultantly, the oligomer chain forms a left-handed α-helix. Three of these helixes form the quaternary structure of collagen, known as tropocollagen [22], which has a molar mass around 300 kDa. This structural protein is a main component of connective tissues in bones, tendons, cartilage, and muscles [23].

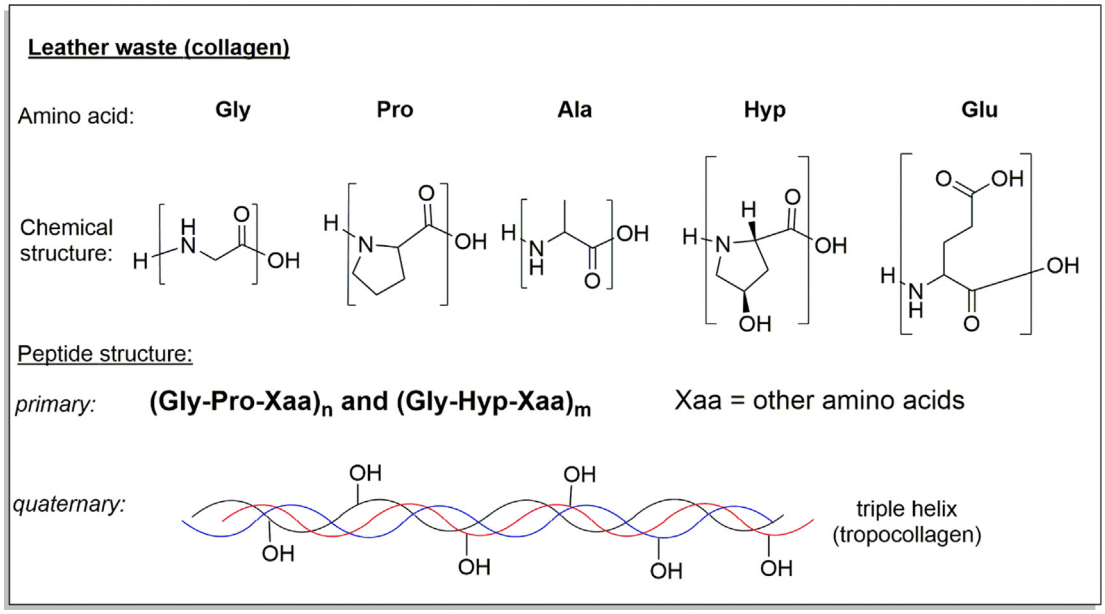

Fig. 1. Leather waste material composition. Three-letter symbols [20] of amino acids in collagen, sorted by relative abundancy [21], and their chemical structures. Primary and quaternary peptide structure (tropocollagen).

Several scientific works are currently underway, focusing on environmental matters caused by the tannery industry wastes, mainly because the most common employed tanning agents are chromium salts [24]. Notedly, tanned leather is also obtained using aluminum or vegetable tanning agents, which is then called white leather.

Wet-white leather waste was collected during the leather shaving step from a local tannery industry in Mexico. LW was ground using a grinder Pagani 20,030 FA model, with 7.5 HP and a 5 mm mesh. Afterwards, LW was dried at 80 °C for 12 h in an oven before the extrusion process. The copolymer of ethylene vinyl acetate (EVA), with an 18% vinyl acetate content and a 2.5 g/10 min melt flow rate, was purchased from Dupont as Elvax® 460. Ammonium polyphosphate (APP) (Exolit® AP422) with 31–32 wt-% phosphorus content and an average particle size D50 of 17 μm, as well as ammonium polyphosphate encapsulated with melamine resin (eAPP) (Exolit® AP462), with 29–31 wt-% phosphorus content and an average particle size D50 of 20 μm, were supplied from Clariant GmbH. The reduced phosphorus-content of eAPP corresponds to the melamine encapsulation. Maleic anhydride (MAH) with 99.0 % purity and benzoyl peroxide (BPO) were purchase from Sigma Aldrich.

In total, eight EVA materials were compared: one was pure EVA, and another a composite of EVA with 10 wt-% leather waste (EVA/LW10). Four samples compared varying loadings (20 – 30 wt-%) of flame retardant (FR) types. Here, conventional APP was compared to melamine-encapsulated APP (eAPP). Finally, two samples that contained both LW and FR were prepared and investigated. An overview is presented in Table 1.

The investigated materials were prepared by extrusion process in a twin-screw extruder (Leistritz Micro 27), L/D = 32, 27-mm diameter with 8 heating zones (Z_1-Z_8), using counter-rotating intermeshing mode, 120 RPM rotational speed and temperature profile, as follows: Z_1 = 137, Z_2 = 157, Z_3 = 165, Z_4 = 170, Z_5 = 175, Z_6 = 180, Z_7 = 185, Z_8 = 185 °C (from feeding zone to die).

Previous studies have pointed out that to produce polymer composites using leather industrial-waste as reinforcement, it is fundamental to improve the compatibility filler-polymer matrix [9–11]. Thus, benzoyl peroxide (BPO) was used as initiator to carry out a grafting reaction of maleic anhydride (MAH) in ethylene segment of EVA during the extrusion process. This was done with the aim of increasing the compatibility of EVA with LW by means of the reaction of grafted MAH with hydroxyl and/or amine groups of the amino acids found in collagen [25]. MAH was been investigated as a grafting agent for PBT/EVA [26] and PETG/EVA blends [27], and a reaction mechanism was been proposed. These investigations highlight the ability of MAH with BPO to act as grafting agent between EVA and other polymers. Moreover, other investigations of MAH as a grafting agent in wood powder composites containing EVA reported a chemical interaction of functional groups in

Table 1
Sample IDs and composition in wt.-%.

Sample ID	EVA /wt.-%	Leather waste /wt.-%	APP /wt.-%	eAPP /wt.-%
EVA	100	–	–	–
EVA/LW10	90	10	–	–
EVA/APP20	80	–	20	–
EVA/eAPP20	80	–	–	20
EVA/APP30	70	–	30	–
EVA/eAPP30	70	–	–	30
EVA/LW10/APP20	70	10	20	–
EVA/LW10/eAPP20	70	10	–	20

wood power and MAH [28]; hence, a similar reaction occurs for EVA and LW. A reaction scheme of the grafting reaction of EVA and LW with MAH is proposed in Scheme S1.

Non-grafted LW and LW grafted with MAH in EVA were compared at 10 wt-% loadings to elucidate the efficacy of grafting via MAH as a compatibilizer. For grafted EVA/LW10 containing MAH, 1.5 phr (parts per hundred resin) of MAH and 0.1 phr of BPO were added under the described extrusion process conditions. Results from mechanical properties measurements showed an improvement on tensile strength using MAH as a grafting agent, from 7.3 ± 0.2 for non-grafted EVA/LW to 8.5 ± 0.2 MPa. Moreover, MAH as a grafting agent in EVA did not modify the thermal stability and flame-retardant behavior of EVA/LW10 sample. These results provided evidence for the successful grafting of LW to EVA via MAH. Therefore, for LW-containing samples, BPO and MAH were added during the compounding of materials. BPO and MAH were dissolved in 50 mL acetone (reagent grade), and this solution was added to EVA pellets. Then, LW was incorporated and mixed. For samples containing FR additives, these were added after LW. All components were mixed manually before being fed to an extruder.

Specimens for mechanical properties, flammability and burning behavior evaluation were obtained by injection molding in a Milacron TM55 injection-molding machine with four heating zones (Z_1-Z_4), under the following conditions: temperature profile of Z_1 = 160, Z_2 = 165, Z_3 = 170, Z_4 = 175 °C (from feeding zone to nozzle), 120 bar injection fill pressure, 75 mm/s injection speed and 35 s cooling time.

Tensile properties, tensile strength, Youngs modulus, elongation at break and tenacity, were evaluated following ASTM D638 standard, using a universal testing machine (Instron, Norwood, MA, USA) 5565 model at a crosshead speed of 50 mm min-1 and type I specimen dimensions.

The morphology of LW, APP and EVA-composites were studied using scanning electron microscope (SEM). Micrograph images of gold-coated, freeze-fractured samples were taken on a Zeiss EVO MA 10 scanning electron microscope (Carl Zeiss AG, Oberkochen, Germany). The acceleration voltage was 10 kV. The specimens were sputter coated with a 15 nm layer of gold using a Quorum Q150R ES rotary pumped coater from Quorum Technologies (Laughton, England).EVA and EVA composite samples were prepared by freeze-fracturing in liquid nitrogen to investigate the cross-section fracture. Leather waste, APP and eAPP were used as provided.

Rheological behavior was investigated in a strain-controlled Ares G2 TA-Instrument rheometer (TA-Instrument, Inc., New Castle, DE, USA), using parallel plates of 25 mm diameter and 0.75 mm gap. The rheological tests were carried out at 195 °C under small amplitude oscillatory shear flow (SAOS) in the linear viscoelastic regimen with 1% strain.

Powdered samples of all materials were obtained using a Cryo-Mill (RETSCH GmbH, Haan, Germany).

Thermogravimetric analysis (TGA) measurements were performed on a TG 209 F1 Iris (Erich NETZSCH GmbH & Co. Holding KG, Selb, Germany) using 10 mg of powdered samples. For pure APP and eAPP, 5 mg sample mass was used instead. The specimens were heated from 30 to 900 °C at a rate of 10 K min^{-1} under a nitrogen purge of 30 mL min^{-1}. All measurements were performed in duplicate, unless the standard deviation was greater than 10%, whereupon a third measurement was made.

Evolved gas analysis measurements were conducted on a Tensor 27 FTIR spectrometer (Bruker Corporation, Billerica, MA, USA) connected to the TGA device via a 1.0 m transfer line heated to 270 °C.

Condensed phase decomposition analysis measurements were performed using an FTIR600 hot-stage cell (Linkam Scientific Instruments Ltd., Chilworth, UK) coupled to a Vertex 70 FTIR spectrometer (Bruker Corporation, Billerica, MA, USA). The specimens were prepared using 150 mg potassium bromide and approx. 2 mg of powdered samples. The components were homogenized with mortar and pestle and pressed into platelets of 10 mm diameter using 7 t of pressure. The specimens were heated from 30 to 600 °C at a rate of 10 K min^{-1} under a nitrogen purge of 300 mL min^{-1}.

Reaction-to-small-flame tests included limiting oxygen index (LOI) and Underwriter's UL-94 tests. LOI measurements were conducted on an Oxygen Index device (Fire Testing Technology, East Grinstead, UK) according to ISO 4589–2 using specimens sized 100 mm × 6.5 mm × 3.1 mm. UL-94 measurements were conducted according to IEC 60659-11-10 on specimen sized 125 mm × 13 mm × 3 mm.

Forced flaming measurements were performed according to ISO 5660 using a cone calorimeter (Fire Testing Technology, East Grinstead, UK) on specimens sized 100 mm × 100 mm × 3 mm. The heat flux was 50 kW m^{-2} and the distance to the cone heater was 35 mm. This distance was chosen to prevent the char layer from touching the heat coils. Previous investigations have shown no significant impact on the heat flux distribution between 35 mm and 25 mm [29].

3. Results and discussion

3.1. Material and mechanical properties

3.1.1. Mechanical properties

The mechanical properties of halogen-free flame retarded polymer materials present a significant difference with respect to the polymer matrix due to flame retardant (FR) additive load that is needed to obtain the desired flame retardancy. The mechanical behaviors of flame retarded materials depend mainly on the FR additive loading, the distribution, and dispersion of particles [30–32]. On the other hand, the mechanical properties of natural fibers in polymer composites are influenced by several variables, such as fiber type and content, length and surface treatment of the fibers, processing conditions, among others [33]. Therefore, the improvement of sufficient mechanical properties of flame retarded polymer composites based on halogen-free additives and natural fibers represents an important challenge in materials science. The mechanical properties of leather waste as fire retardant adjuvant in EVA polymer composites is a clear example of this problem.

Table 2 discloses the Young's modulus, tensile strength, elongation at break and tenacity results of the investigated EVA composites. According to Table 2, EVA polymer matrix presented a traditional elastomer behavior: relative low Young's modulus and tensile strength (33 and 8.1 MPa, respectively), high elongation at break (312 %) and tenacity (20 MPa). Certainly, the addition of LW and FR additives modified the mechanical behavior of the materials. When EVA contained 10 wt-% LW (EVA/LW10), the resultant material showed a Young modulus which was about 1.5 times higher than pure EVA. The tensile strength was also slightly increased from 8.1 to 8.5 MPa. The increment of elastic modulus with the addition of 10% LW has been observed in polymer composites using PLA at different LW contents; the authors attributed this behavior to the poor dispersion of the leather fibers [9].

The lack of interaction of polymer to APP particles is evidenced by the increment of Young's modulus and the reduction on elongation at break and tenacity, with respect to the total added load. The composites' stiffness increased not only by the total load added, also for the type of components: EVA/LW10/APP20 and EVA/LW10/eAPP20 composites presented Young's moduli about 2.5–

Table 2
Tensile properties of EVA and leather waste polymer composites.

Sample	Tensile strength /MPa	Young's modulus /MPa	Elongation at break /%	Tenacity /MPa
EVA	8.1 ± 0.1	33 ± 1	312 ± 24	20 ± 2
EVA/LW10	8.5 ± 0.2	48 ± 2	230 ± 10	17 ± 1
EVA/APP20	7.7 ± 0.2	55 ± 1	257 ± 10	17 ± 1
EVA/eAPP20	7.4 ± 0.1	52 ± 1	250 ± 9	16 ± 1
EVA/APP30	7.1 ± 0.2	73 ± 2	224 ± 12	14 ± 1
EVA/eAPP30	6.9 ± 0.1	63 ± 2	219 ± 19	13 ± 1
EVA/LW10/APP20	7.6 ± 0.2	88 ± 7	176 ± 16	12 ± 1
EVA/LW10/eAPP20	7.8 ± 0.1	83 ± 5	167 ± 12	11 ± 1

2.7 times that of EVA, as well as decreased elongation at break (43 and 46% reduction, respectively) and tenacity values (40 and 45% reduction), even though the EVA/APP30 and EVA/eAPP30 composites were compounded at the same total load (30 wt-%). At 30 wt-% FR loadings, the FR types behaved disparate: APP exhibited a proportionally higher Young's modulus (2.2 times greater) than eAPP (1.9 times greater) at equal loadings. Overall, the addition of flame retardants to EVA led to decreased elongations at break and reduced tenacity, caused by increased brittleness of the material. These investigations pointed out that the mechanical properties of EVA/LW10/APP20 and EVA/LW10/eAPP20 were comparable, or in some cases superior, to EVA containing equal loadings of P-FRs, signifying the ability of LW to act as a reinforcing filler.

3.1.2. Morphology

Fig. 2 displays the raw material EVA, the phosphorus flame retardant APP, and LW at two different magnifications. Fig. 2a shows the cross section of EVA; the fracture planes were not well defined and showed no orientation, which exhibits a ductile fracture surface. Fig. 2b highlights that APP particles had an irregular shape: the inorganic crystals had a diameter of approximately 12–25 μm. Fig. 2c and Fig. 2d illustrate that LW fibers exhibited heterogenous lengths and widths; some had a diameter up to 160 μm and a length up to 3 mm. Fig. 2d displays a smooth surface along the fiber and a rough surface at the end of the fiber, which is consistent with the fibril structure of collagen: it consists of many collagen microfibers that are bound in a longitudinal arrangement. At the end of one fiber, the bundle of microfibers split, resulting in a rough surface structure.

Fig. 3 shows pure EVA (Fig. 3a) in comparison to EVA composites EVA/LW10 (Fig. 3b), EVA/APP30 (Fig. 3c), and EVA/LW10/APP20 or EVA/LW10/eAPP20 (Fig. 3d and Fig. 3e). The fracture surface of EVA/LW10 is shown in Fig. 3b: the fracture planes were more clearly defined compared to EVA, but they were much larger in comparison to EVA/APP30 (Fig. 3c). The fibers contributed to a higher Young's modulus, meaning a stiffer material; this behavior is shared by many other fibrous fillers or additives. The fiber in the micrograph (green area of Fig. 3b) was ripped during the fracture. No interstices were observed around the fibers, indicating that the fiber was well embedded in the polymer matrix. The cross-section surface of EVA/APP30 had many small and well-defined fracture planes. The APP particles were well dispersed throughout the polymer matrix, no agglomeration of the particles was observed. The high APP loading led to a brittle material, which was characterized by well-defined fracture planes; this phenomenon aligns with the results of mechanical measurements

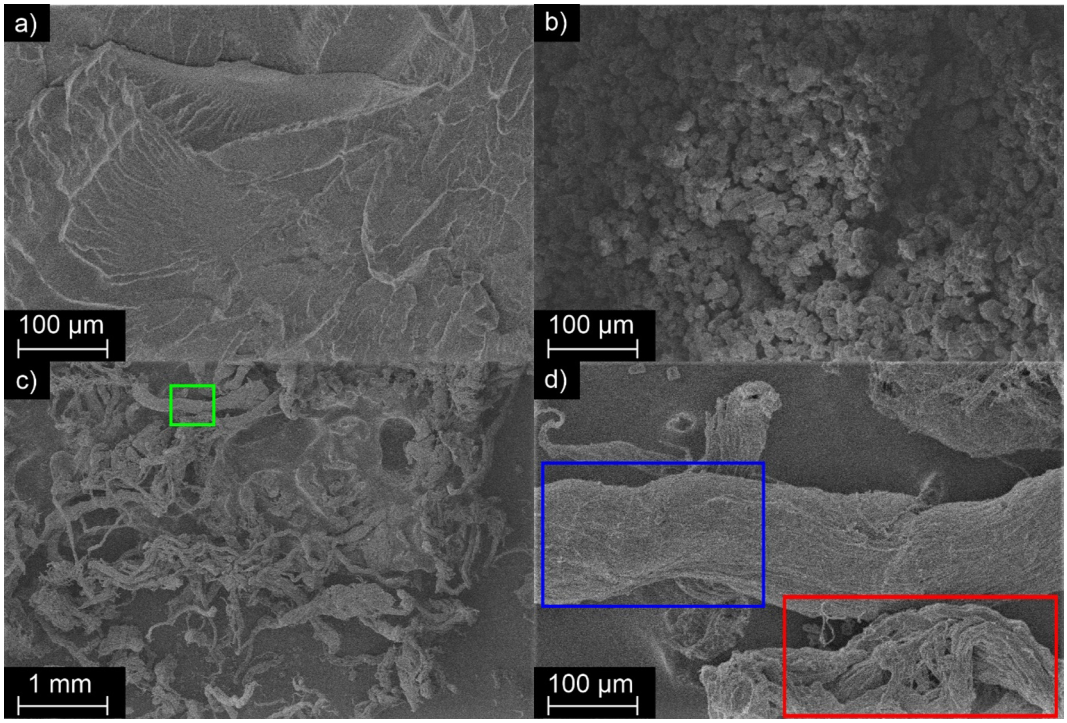

Fig. 2. SEM Micrographs of EVA and additives to EVA composites. a) EVA; b) APP; c) LW fibers; d) Close-up of the green section in c) showing the smooth fiber surface (blue) and the rough end of a fiber (red). (For interpretation of the references to colour in this figure legend, the reader is referred to the web version of this article.)

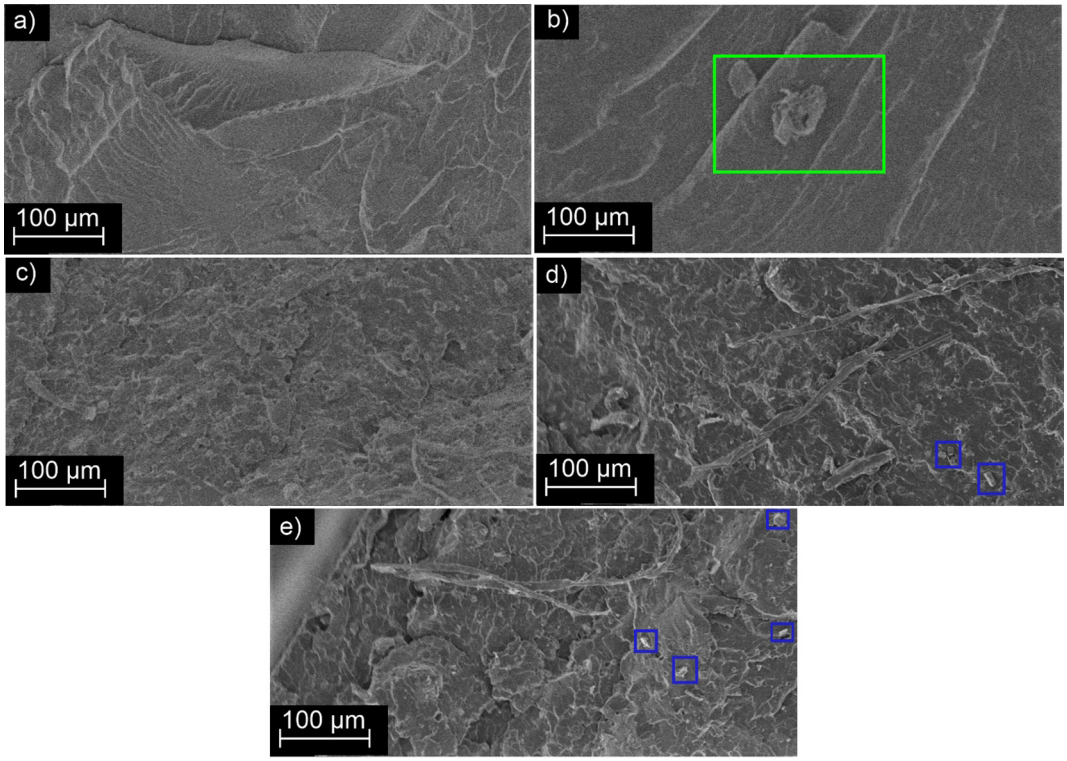

Fig. 3. SEM micrographs of EVA and EVA composites. a) EVA; b) EVA/LW10 (LW fiber in green box); c) EVA/APP30; d) EVA/LW10/APP20; e) EVA/LW10/eAPP20. Green box: LW fiber; blue box: APP or eAPP particles. (For interpretation of the references to colour in this figure legend, the reader is referred to the web version of this article.)

(Table 2), which showed a higher Young's modulus for EVA/APP30 (73 MPa) compared to EVA (33 MPA). Fig. 3d and Fig. 3e depict the SEM micrographs for EVA/LW10/APP20 and EVA/eAPP20/LW10. Like EVA/APP30, the EVA/LW10/APP20 composite (Fig. 3d) showed many small fractural planes. The APP particles were well dispersed, an agglomeration of particles was not detected. No significant changes were observed when eAPP was used in EVA/eAPP20/LW10 (Fig. 3e) compared to EVA/LW10/APP20. Although improving the interfacial interaction between APP particles and EVA/LW was not the aim of this study, studies have illustrated the significance of such interaction between APP and matrix, showing improved flame retardancy due to the formation of phosphorus-moieties along the interfaces [34].

3.1.3. Rheology

The flow behaviors of EVA and EVA composites were investigated under small amplitude oscillatory shear flow (SAOS). Fig. 4a depicts the complex viscosity and Fig. 4b depicts the storage modulus as a function of angular frequency. According to the plotted data in Fig. 4a, EVA and EVA composites showed a pronounced shear thinning behavior, the complex viscosity decreased with respect to angular frequency increases. On the other hand, complex viscosity magnitude increased with LW and FR-additives loadings. The increment depends mainly on the load amount; EVA composites with 30 wt-% total loading (namely, EVA/APP30, EVA/eAPP30, EVA/LW10/APP20 and EVA/LW10/eAPP20) exhibited increased complex viscosity over the whole frequency range. Interestingly, the complex viscosity of EVA using 10 wt-% LW (EVA/LW10) was nearly identical to that EVA loaded with 20 wt-% FR-additives (EVA/APP20 or EVA/eAPP20). This behavior was associated to the presence of LW bundles which were not well separated; these macromolecules have a more long-distance effect than particles and therefore restrict the mobility of polymer chains, making their orientation toward flow direction more difficult. The small APP and eAPP particles at 20 wt-% were better oriented to the flow direction, and this effect has been observed in other polymer systems using natural fibers at different size [17].

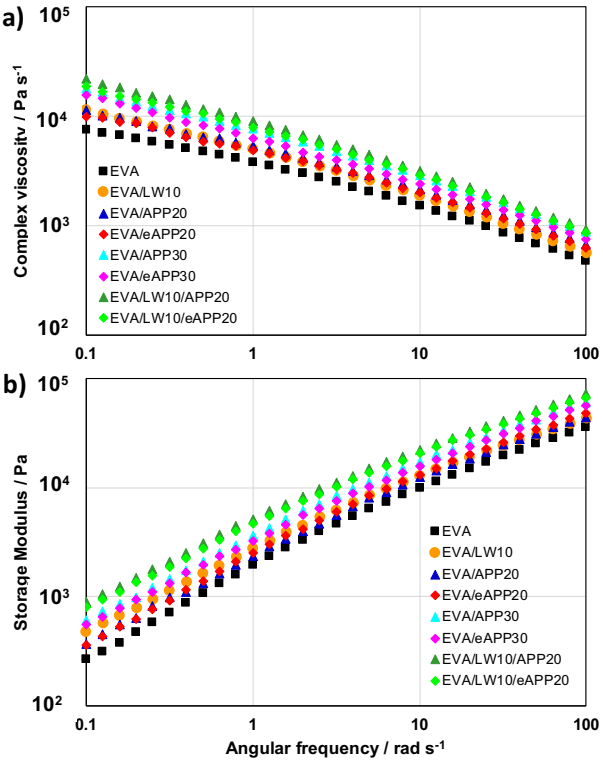

Fig. 4. a) Complex viscosity and b) storage modulus as a function of angular frequency.

Fig. 4b plots the storage modulus with respect to angular frequency for EVA and EVA composites. The reported data indicated that the elastic behavior of the composites was enhanced with the addition of LW and FR-additives. The storage modulus values increased compared to the EVA values in the whole frequency range, following the same pattern of EVA, i.e., the storage modulus curves showed a similar slope. The elastic behavior of the composites was highly dependent on the materials composition: 10 wt-% LW produced comparable elastic behavior than 20 wt-% APP or eAPP; this occurred in particular at the high frequency range (10–100 rad s^{-1}) where the EVA/LW10, EVA/APP20 and EVA/eAPP20 curves overlapped. At low frequencies (0.1–1 rad s^{-1}), EVA/LW10 showed higher storage modulus values than EVA/APP20 and EVA/eAPP20 composites: indeed, the increment is similar to that presented by EVA/APP30 and EVA/eAPP30. This effect was observed over the entire frequency range for samples containing LW and FR-additives: EVA/LW10/APP20 and EVA/LW10/eAPP20 curves exhibited increased storage modulus compared to all other samples. The long distance effect of the LW fibers was evidenced in the increment on storage modulus, in particularly at the low frequency range (0.1–1 rad s^{-1}), suggesting somewhat good interactions between collagen fibers and EVA, as it has been proposed for EVA polymer nanocomposites, where good distribution and dispersion of the nanoparticles were achieved [35]. The rheological measurements pointed out that LW and FR- additives were well distributed and dispersed during processing, therefore the standard processing conditions applied to EVA could be used for the flame retarded EVA composites.

3.2. Pyrolysis investigation

The pyrolytic decomposition of the individual additives LW, APP, and eAPP, as well as all EVA composites were investigated by thermogravimetric analysis (TGA). The evolved gas was analyzed using an FTIR coupled to the TGA (TG-FTIR), and the condensed phase FTIR was investigated via hot-stage FTIR. These tests were chosen to characterize the fire behavior, as fire tests like UL-94, LOI, and cone calorimeter measurements rely on a diffusion flame and an anaerobe decomposition in the pyrolysis zone [36–38]. Hence, pyrolytic thermogravimetric decomposition in the gas and condensed phase were chosen to complement fire tests.

3.3. Thermogravimetric analysis (TGA)

The results of TGA measurements are summarized in Table 3 and are shown in Fig. 5, where the mass loss and mass loss rate are displayed as a function of temperature. The mass loss curves in Fig. 5 highlight the decomposition of pure leather waste, which exhibited a water content of about 9 wt%, illustrated by the initial mass loss seen below 100 °C. The main decomposition step of leather waste occurred at 327 °C. Fig. 5a and Fig. 5b illuminate that EVA and EVA composites showed similar decomposition behavior: all mass loss curves of EVA composites exhibited a two-step decomposition beginning at about 350 °C (T_1) and peaking at 473 °C (T_{max}). Notably, T_1 was higher and the corresponding mass loss (ML_1) was greater for EVA samples that contained LW. The mass loss of the main decomposition step (ML_{max}) was low for EVA-FR (APP or eAPP) composites, however the residue amount decreased steadily with increasing temperature and dropped above 700 °C, implying that the formed residue was only moderately thermally stable. In contrast, EVA/LW10/APP20 and EVA/LW10/eAPP20 exhibited more thermally stable residues, and their residue yields were significantly higher than other EVA composites.

The measured residue for EVA/LW10 was lower than the calculated theoretical value. This phenomenon is explained by the lack of interaction between LW and EVA during decomposition: LW decomposes at a lower temperature than EVA; more specifically, the T_{max} of LW is below $T_{5\%}$ of EVA. EVA with P-FRs APP or eAPP exhibited higher residue yields than their calculated values, indicating a meaningful interaction in the condensed phase between matrix and flame retardant. APP-containing composites retained higher residues than those containing eAPP, they also exceeded their calculated residues by a higher margin. The samples EVA/LW10/APP20 and EVA/LW10/eAPP20 displayed not only a higher measured residue yield than their calculated values, but the overall residue yields were greater (28% and 22%, respectively) than equal loadings of P-FRs, highlighting that LW acted as an adjuvant to APP or eAPP in EVA.

3.4. Evolved gas analysis (TG-FTIR)

The evolved gas of the pyrolytic decomposition of EVA was analyzed by TG-FTIR, and Fig. S1 displays the spectra recorded at T_1 and at T_{max}. The spectra in Fig. S1a and Fig. S1b highlight that the decomposition products of EVA were the most prevalent products in the evolved gas spectra of EVA composites. The two decomposition steps seen in the TGA spectra of EVA (Fig. 5a) correspond to the two-step decomposition of the ethylene–vinyl acetate backbone, where the deacetylation of the vinyl acetate groups occurs at T_1, followed by the decomposition of the polymer backbone at elevated temperatures T_{max} [39]. The spectrum of EVA in Fig. S1a exhibited a strong band at 1791 cm^{-1} from the C=O stretching vibration of the carboxyl groups, more closely of acetates or anhydrides formed during the deacetylation reaction. The main pyrolysis products at T_1 were carbon dioxide (approx. 2200 cm^{-1}), water

Table 3
Results from thermogravimetric analysis measurements.

Sample	$T_{5\%}$ /°C	T_1 /°C	ML_1 /wt.-%	T_{max} /°C	ML_{max} /wt.-%	Residue (800 °C) /wt.-%	Calculated residue /wt.-%
Leather waste	83 ± 5	80 ± 2	9 ± 1	327 ± 2	61 ± 1	25.7 ± 0.7	–
APP	313 ± 2	317 ± 1	15 ± 2	592 ± 1	61 ± 5	16.3 ± 2.7	–
eAPP	316 ± 2	330 ± 10	20 ± 0	607 ± 38	52 ± 10	17.8 ± 3.3	–
EVA	344 ± 0	349 ± 4	13 ± 0	473 ± 0	87 ± 0	0.1 ± 0.1	–
EVA/LW10	322 ± 3	353 ± 4	17 ± 1	473 ± 1	79 ± 1	2.1 ± 0.4	2.8
EVA/APP20	346 ± 1	356 ± 0	13 ± 0	475 ± 1	74 ± 0	4.6 ± 0.8	2.9
EVA/eAPP20	343 ± 0	355 ± 0	13 ± 0	475 ± 1	76 ± 0	7.6 ± 0.7	4.4
EVA/APP30	347 ± 2	358 ± 0	12 ± 0	475 ± 1	66 ± 1	7.6 ± 0.7	5.0
EVA/eAPP30	345 ± 0	356 ± 4	13 ± 0	475 ± 1	68 ± 1	7.1 ± 0.3	5.5
EVA/LW10/APP20	319 ± 1	351 ± 6	17 ± 0	474 ± 2	66 ± 1	9.7 ± 0.3	6.0
EVA/LW10/eAPP20	318 ± 2	351 ± 1	18 ± 0	474 ± 0	66 ± 0	9.3 ± 0.6	6.3

$T_{5\%}$: temperature at 5% mass loss; T_1: temperature of 1st decomposition step (local maximum mass loss); ML_1: mass loss of T1; T_{max}: temperature of main decomposition step (maximum mass loss); ML_{max}: mass loss of T_{max}.

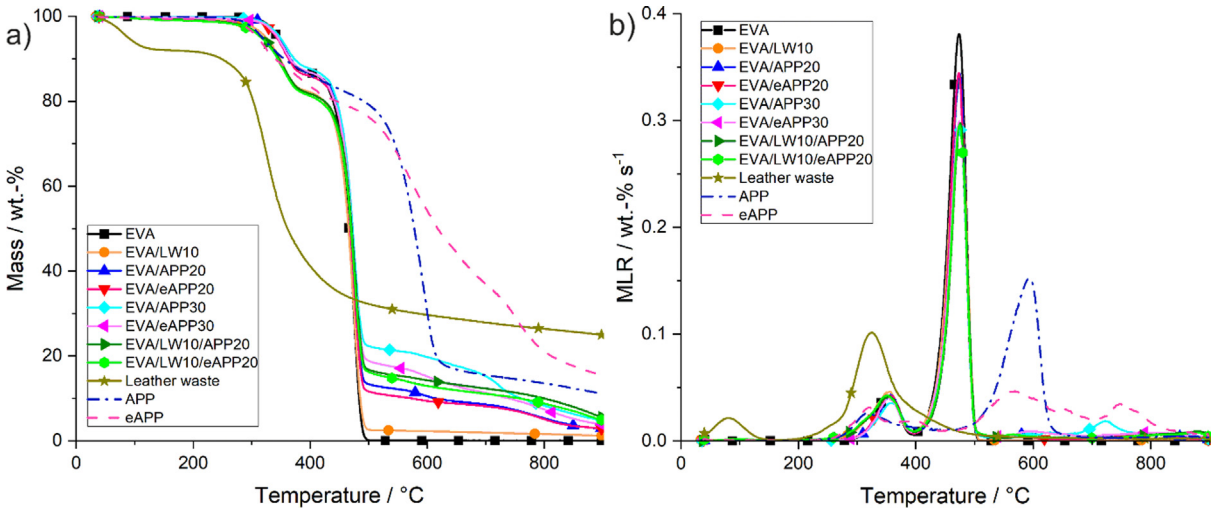

Fig. 5. a) Mass loss and b) mass loss rate as functions of temperature from thermogravimetric analysis measurements.

(between 4000 and 3500 cm^{-1}), and ammonia, confirmed by the two bands at 965 and 930 cm^{-1}. The second decomposition step, displayed in Fig. S1b, illustrates the presence of aliphatic hydrocarbons via the two bands at 2930 and 2854 cm^{-1} corresponding to ν (C-H) vibrations. The band at 1461 cm^{-1} is linked to δ(C-H). Notably, at T_{max} the EVA/LW10/APP20 and EVA/LW10/eAPP20 exhibited some bands corresponding to decomposition products from leather waste, particularly ammonia, carbon dioxide, and water. These bands were not detected at T_{max} in EVA samples with FR.

3.5. Condensed phase analysis via hot-stage FTIR

The condensed phase FTIR spectra from hot stage measurements at varying decomposition stages are presented in Fig. S2. The three spectra correspond to the materials at three distinct temperatures, namely before T_1 (at 240 °C), after T_1 and before T_{max} (at 395 °C), and at 600 °C. Fig. S2a displays that EVA/LW10 exhibited a distinct band at 1147 cm^{-1} which was not present in pure EVA. This band corresponds to anhydride signals (R-(C=O)-O-(C=O)-R), or various R-O-(C=O)-R signals [40]. These signals are resultant from the grafting reaction of LW with maleic anhydride. Moreover, the band at 1666 cm^{-1} was visible in EVA/LW10 as well as EVA/LW10/APP20 and EVA/LW10/eAPP20; it can correspond to aldehydes, β-ketoaldehydes as enols, or primary amide (R-(C=O)-NHR) signals, indicating the presence of amino acids. The thermal degradation of EVA is marked by the deacetylation of the pendant group. In Fig. S2b, the presence of the band at 1099 cm^{-1} in EVA and EVA/LW10 corresponds to ν_s(C-O) from saturated secondary alcohols [41]. The changes in this band after T_1 are the result of deacetylation, which is the primary mechanism in the first decomposition step. The bands in all APP or eAPP containing samples exhibited the presence of phosphates from APP. Fig. S2c exhibits the fingerprint region of all composites at 600 °C. The highlighted bands correspond to various P, P—O, P—N, and P—C bonds, which provides evidence of the formation of a phosphorus, nitrogen, and carbon rich residue. The signals have been examined in detail in previous studies of phosphorus and nitrogen containing flame retardants [42]. Notable bands are 1400 cm^{-1} (P-CH_2-R, or P-Phenyl, or P=N, or P-N-Ph), 1292 and 1274 cm^{-1} (P=O, or P-CH_3), as well as 1155 cm^{-1} (P-O-C_{arom}) and 1099 cm^{-1} (P-C_{arom}) [43]. Notably, in Fig. S2c the shapes of the signals at 1099 cm^{-1} and 518 cm^{-1} (C-C skeletal) are different between samples EVA/APP20 or EVA/eAPP20 and EVA/LW10/APP20 or EVA/LW10/eAPP20, which implies a varying chemical surrounding for these signals for materials that contain LW and flame retardants. Moreover, the bands at 1010 and 742 cm^{-1} were visible for EVA/LW10/eAPP20, which may correspond to ureas or aromatic hydrocarbons, which illustrates the enhanced condensed phase interaction of eAPP in the composites. These results provide evidence for the residue enhancing effect that LW had on the pyrolytic decomposition of flame retarded EVA. Moreover, the residues from EVA/LW10/APP20 and EVA/LW10/eAPP20 were very similar to EVA/APP20 and EVA/eAPP20 because the signals from APP were very predominant. All samples contain various P-signals, showing that EVA interacted with APP via phosphorylation and the formation of P-N-containing residues.

4. Fire testing

4.1. Reaction-to-small-flame tests

To gain insight into the flammability behavior of EVA and its composites, two reaction-to-small-flame tests were performed, namely limiting oxygen index (LOI) and UL-94 test in vertical orientation. The results of both measurements are summarized in Table 4. EVA and EVA/LW10 did not achieve UL-94 rating; the specimens burned longer than a total of 60 s, they showed burning drips, and burned to the clamp. Compared to EVA, EVA/LW10 decreased the LOI slightly from 22.3% to 21.2%. All samples that contained either APP or eAPP as a flame retardant achieved a V-2 rating. EVA/APP20 showed a slight increase in LOI-value compared to EVA (LOI = 24.8%, increase of 2.5 vol-%), which was similar to EVA/APP30 (LOI = 24.5%). Thus, elevated APP loadings did not improve the LOI of EVA samples, because the flame-retardancy potential of FRs like APP is not linear to its loading; the performance levels off after at a certain concentration [44]. For eAPP,

Table 4
Results from reaction-to-small-flames tests (UL-94, LOI).

Sample	UL-94 rating	LOI/vol.-% [O_2]
EVA	NR	22.3 ± 0.2
EVA/LW10	NR	21.2 ± 0.2
EVA/APP20	V-2	24.8 ± 0.2
EVA/eAPP20	V-2	23.8 ± 0.2
EVA/APP30	V-2	24.5 ± 0.3
EVA/eAPP30	V-2	23.9 ± 0.2
EVA/LW10/APP20	V-2	24.1 ± 0.1
EVA/LW10/eAPP20	V-2	24.9 ± 0.2

nearly no difference was observed between 20% and 30% eAPP content in EVA. The results show that for reaction-to-small-flame tests, the increase of FR content had no added effect on UL-94 or LOI rating.

Although the LOIs of samples containing only FR-additives were almost equal to those containing both LW and FRs, a difference in burning behavior was observed. In UL-94, instead of continuous dripping, the sample burned until the lower part of the polymer dropped off and was removed from the specimen; a char layer was formed and the bottom end of the specimen. This layer acted as a thermal barrier and prevented upward flame spread, and it promoted extinguishment by dripping. To compare the sample residues after LOI tests, EVA/LW10/eAPP20, EVA/LW10/APP20, and EVA/APP20 are shown in Fig. 6. EVA/LW10/eAPP20 formed a stable protective char layer around the top. EVA/LW10/APP20 showed some formation of intumescent char and the specimen remained in an upward position, while the EVA/APP20 specimen bent and melted.

As several investigations on multicomponent polymer composites with organic fillers and flame retardants have identified, the interaction of polymer, filler, and flame retardant during flaming combustion can lead to enhanced fire performance of the blend [16,17,45]. The chemical interaction of the FRs APP and eAPP with the EVA matrix was apparent from the reaction-to-small-flame measurements. The results of EVA/LW10 were consistent with TGA measurements, where this sample exhibited low residue yields. LW as a single additive in EVA showed little flame retardancy value, yet its presence enhanced the flame retardancy of FR-containing EVA composites via char formation. LW enhanced both the pyrolytic decomposition and the burning behavior of flame retarded EVA composites: EVA composites containing 10 wt-% LW + 20 wt-% FR-additives exhibited more effective flame retardancy in terms of flame inhibition and increased residue formation than EVA samples containing 30 wt-% FR loadings. The combination of LW and FR-additives in EVA enhanced the condensed phase mode of action, leading to a slightly increased LOI and enhanced residue morphology.

4.2. Forced flaming combustion tests

The forced flaming behavior of EVA and EVA composites with LW and FRs was investigated using a cone calorimeter, and Table 5 summarizes the results of these measurements, while Fig. 7 exhibits the heat release rates (HRR) and total heat releases (THR) as a function of time. Fig. 7a plots the HRRs of EVA and EVA composites as a function of time. EVA/LW10 exhibited higher peaks of heat release rates (PHRR) than pure EVA. This is explained by the decomposition of LW, which occurred at a lower temperature (about 100 °C) than the matrix, as seen in TGA results. While volatile decomposition products of LW contributed to the HRR to some degree, the increase in HRR is explained by the decomposition of LW accelerating the combustion of EVA. This point is strengthened when comparing the total heat evolved (THE) of both EVA and EVA/LW10: the overall fire load both materials are almost identical.

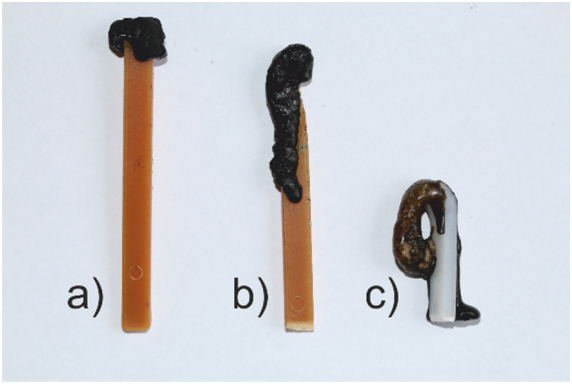

Fig. 6. LOI specimens after testing; a) EVA/LW10/eAPP20 b) EVA/LW10/APP20 and c) EVA/APP20.

All APP or eAPP-containing EVA samples exhibited a lower PHRR and THE than pure EVA. The decrease of PHRR is explained by the formation of a protective layer which retained fuel in the condensed phase; this also resulted in a lower fire load. Moreover, the effective heat of combustion (EHC) of some APP or eAPP composites were lower compared to EVA, implying a minor gas phase effect caused by fuel dilution from the release of ammonia, as well as radical scavenging, as lower EHC values are an indicator of this mode of action of phosphorus [46]. The incorporation of higher FR-loadings was only effective for eAPP when comparing results from EVA samples with 20 and 30 wt-% loadings; this phenomenon is linked to the increased ammonia production of 30 wt-% eAPP. Higher APP loadings did not greatly alter the fire behavior: residue amounts increased and the PHRR was lowered.

EVA/LW10/APP20 and EVA/LW10/eAPP20 exhibited an improved fire performance compared to EVA and EVA with only P-FRs, as evidenced by decreased values for PHRR, THE, EHC, and MARHE. The PHRRs of EVA/LW10/APP20 and EVA/LW10/eAPP20 were lower than any other EVA composite: they were reduced by more than 50% compared to pure EVA. Moreover, the change in curve shape signifies the formation of a charring residue [47,48]; this residue acted as a protective layer and thermal barrier, which retained fuel in the condensed phase and depressed HRRs. These results mirror previous investigations of P-FRs and organic fillers in EVA, where cyclodextrins interacted with APP in EVA to reduce PHRR via the improvement of the protective layer [49]. This phenomenon was visually assessed during fire tests via the formation of char at the top of the burning sample; moreover, the residues after cone calorimeter measurements also reveal the difference in char formation of EVA/LW10/APP20 and EVA/LW10/eAPP20 compared to other EVA composites. Although 30 wt-% FR-loadings in EVA composites led to higher residue yields for EVA/APP30 and EVA/eAPP30 compared to EVA/LW10/APP20 and EVA/LW10/eAPP20, it is not char yield alone, but residue morphology, properties, and formation which are most relevant to improving the flame retardancy of polymeric materials [46]. This point is strengthened when comparing THE values, where EVA/LW10/APP20 and EVA/LW10/eAPP20 exhibited reduced THE values compared to other EVA composites; compared to pure EVA, the fire load was decreased by about 20%, and by 5% and 1% compared to equal P-FR loadings in EVA, respectively. THE is related to the combustion efficiency (χ), the heat of combustion of the volatiles (h_c^0), the mass loss (m_0) and the char yield (μ) via the following equation [44,47]:

$$THE \propto \chi\, h_c^0 (1-\mu)\, m_0 \tag{1}$$

Thus, the reduction in THE of EVA/LW10/APP20 and EVA/LW10/eAPP20 compared to EVA/APP30 and EVA/eAPP30 is explained by a reduction in the effective heat of combustion $\chi\ h_c^0$, especially because fuel reduction (1-μ) was more pronounced for EVA/APP30 and EVA/eAPP30, which attained higher residue yields. Table 5 shows that the EHC values of EVA/LW10/APP20 and EVA/LW10/eAPP20 were most reduced among EVA composites (20% and 19% compared to EVA, respectively); the reduction in EHC for EVA/LW10/APP20 and EVA/LW10/eAPP20 compared to EVA/APP30 and EVA/eAPP30 (11% and 7%, respectively) is explained by a reduction in χ, as well as fuel dilution effects affecting h_c^0. Moreover, a reduction in combustion efficiency leads to more

Table 5
Results from forced flaming combustion tests via cone calorimeter.

Sample	EVA	EVA/LW10	EVA/APP20	EVA/eAPP20	EVA/APP30	EVA/eAPP30	EVA/LW10/APP20	EVA/LW10/eAPP20
t_{ig}/s	36 ± 1	23 ± 1	32 ± 1	30 ± 2	35 ± 1	28 ± 5	29 ± 1	29 ± 1
PHRR/kW m^{-2}	962 ± 94	1505 ± 25	758 ± 11	688 ± 2	780 ± 25	565 ± 8	466 ± 2	448 ± 39
THE/MJ m^{-2}	112.3 ± 5.8	108.1 ± 0.2	96.5 ± 0.5	96.7 ± 0.7	95.6 ± 0.8	93.3 ± 0.1	90.9 ± 2.2	92.4 ± 4.7
Residue/wt.-%	0.8 ± 0.4	1.2 ± 0.7	15.5 ± 0.3	11.7 ± 1.5	21.5 ± 0.4	21.5 ± 0,5	16.6 ± 0.1	16.4 ± 0.1
EHC/MJ kg^{-1}	38.8 ± 2.0	35.9 ± 0.3	34.7 ± 0.2	33.2 ± 0.4	35.0 ± 0.1	33.9 ± 0.4	31.2 ± 0.8	31.6 ± 1.6
MARHE/kW m^{-2}	562 ± 27	605 ± 13	446 ± 7	439 ± 2	436 ± 1	383 ± 12	349 ± 5	330 ± 25
TSP/m^2	12.5 ± 0.8	10.9 ± 0.4	16.2 ± 0.2	17.4 ± 0.7	15.0 ± 0.9	15.9 ± 0.6	20.9 ± 0.6	20.5 ± 0.1
av-COY/10^2 kg kg^{-1}	3.9 ± 0.2	3.5 ± 0.1	5.6 ± 0.0	5.8 ± 0.0	5.2 ± 0.1	5.3 ± 0.1	6.8 ± 0.1	7.6 ± 0.5
FRI/–	–	0.43	1.34	1.37	1.44	1.59	2.12	2.17

t_{ig}: time to ignition; PHRR: peak of heat release rate; THE: total heat evolved (fire load); EHC: effective heat of combustion; MARHE: maximum average rate of heat emission; TSP: total smoke production; av-COY: average carbon monoxide yield; FRI: flame retardancy index.

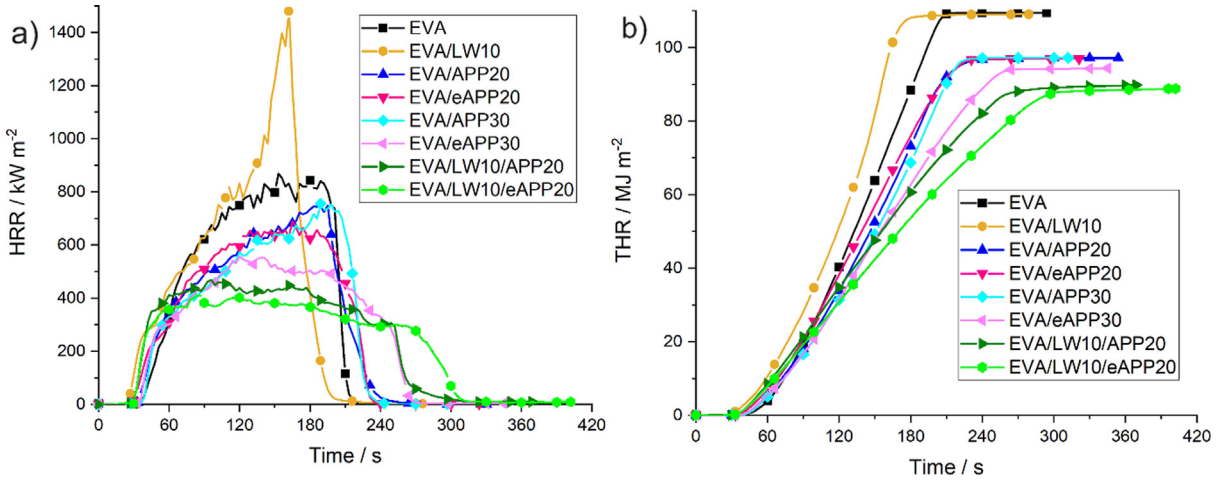

Fig. 7. Forced flaming combustion tests via cone calorimeter; a) heat release rate, and b) total heat release as functions of time.

incomplete combustion, the result of which is increased smoke production: for EVA/LW10/APP20 and EVA/LW10/eAPP20, the total smoke production (TSP) was increased by a factor of 1.7 and 1.6, respectively, compared to EVA, and by a factor of 1.4 and 1.3, respectively, compared to 30 wt-% loadings of FR. This phenomenon is also coupled to an increase in the average carbon monoxide yield during burning (av-COY) as a product of incomplete combustion: notably, this trend is visible for APP or eAPP containing and especially for LW and FR-containing composites, where av-COY of EVA/LW10/eAPP20 is 1.96 times greater than EVA, and 1.43 times greater than EVA/eAPP30. Furthermore, the heat release rate as a function of time (HRR(t)) is defined by:

$$HRR(t) \propto \theta(t)\chi h_c^0(1-\mu) \quad (2)$$

An empirical factor for the protective layer is given by ($\theta(t)$). As THE $\propto$ HRR(t), the reduced fire load of EVA/LW10/APP20 and EVA/LW10/eAPP20 compared to other EVA composites is related to the protective layer effect $\theta(t)$, which was pronounced for these materials. The decrease in fire load and PHRR implies that LW and FR-additives had a synergistic effect on these values, as the combination of these two compounds attained a better fire performance than either single compound in EVA composites. This point is further strengthened by comparing the values of the maximum average rate of heat emission (MARHE) of all materials. MARHE is used in fire protection of railway vehicles (CEN TS 45545) and is used as an index for fire performances. Notably, EVA/LW10/APP20 and EVA/LW10/eAPP20 exhibited a 20% and 14% reduction in MARHE values compared to equal loadings of P-FRs in EVA, respectively, and the MARHE was reduced by about 40% compared to pure EVA.

One way of visualizing the flame retardancy effect is via Petrella plot, where the fire load (THE) is plotted as a function of the fire growth index (PHRR/t_{ig}) [50]. Fig. 8 displays the Petrella plot for EVA and EVA composites; an improvement in fire behavior is characterized by a shift to the lower left corner of the plot, i.e., a reduction in both THE and PHRR/t_{ig}. Starting from pure EVA (black square in Fig. 8), the incorporation of LW (EVA/LW10) slightly reduced THE, but greatly increased the fire growth index, while

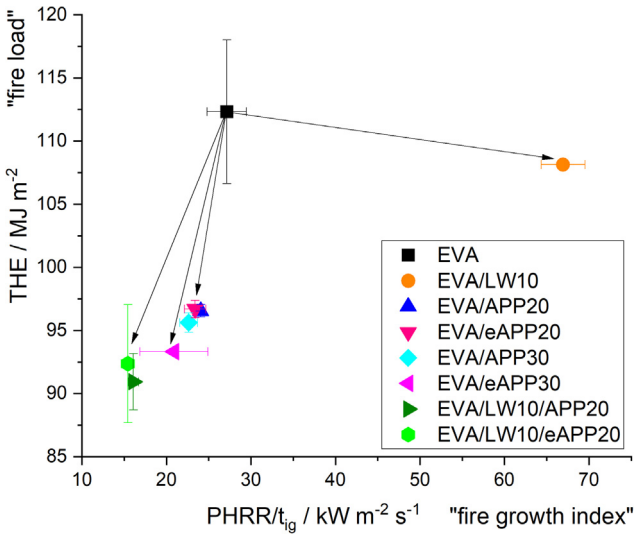

Fig. 8. Petrella plot of EVA and EVA composites.

the addition of 20 or 30 wt-% FR-additives lowered both THE and PHRR/t_{ig}. Fig. 8 illustrates that EVA/LW10/APP20 and EVA/LW10/eAPP20 exhibited a reduction of both fire load and fire growth index compared to EVA/APP30 and EVA/eAPP30 and especially compared to pure EVA. These result points to a high synergy with respect to lowering fire load.

A method of quantifying flame retardancy is by calculating the flame retardancy index (FRI), which is a dimensionless value that evaluates the ratio of the products of fire load and fire growth index of the polymer and its composites [51]. EVA/LW10 exhibited a low FRI value (<1), which suggests that the additive did not enhance the flame retardancy of EVA. The composites containing 20 or 30 wt-% FR showed FRI values between 1.3 and 1.6, yet the combinations containing both LW and APP or eAPP exhibited the highest values at 2.1 and 2.2, respectively, further indicating that LW acted as an adjuvant to APP and eAPP in EVA.

The synergy between LW and the FR-additives in EVA can be quantified using a synergistic effect index (*SE*); this quantification has been described previously [52,53], also for fibers in flame retarded polymers [45]. The quantification of synergy in flame retardant polymers was proposed by Weil [54] and Lewin [55], and commented recently [38]: Two components are synergistic when the combination leads to a superior effect (*SE* greater than 1) compared to the superposition of the individual components; if *SE* < 1, the two components are antagonist. The synergy of LW and FR-additives was quantified according to the method described by Wu et al. [56], using the following equation using THE as an example:

$$SE_{rel}{}^{(1)} = \frac{1 - \frac{THE(EVA+xLW+yFR)}{THE(EVA)}}{1 - \frac{THE(EVA+xLW)}{THE(EVA)} \times \frac{THE(yFR)}{THE(EVA)}} \quad (3)$$

Here, the *SE* was calculated as the relative change of THE, where *x* was the loading of LW and y the loading of FR-additives in wt.-%. Another method proposed by Wu et al. calculates *SE* with respect to equal filler contents according to the following equation:

$$SE_{rel}{}^{(2)} = \frac{1 - \frac{THE(EVA+xLW+yFR)}{THE(EVA)}}{1 - \frac{THE(EVA+xLW)}{THE(EVA)} \times \left(1 - \left(1 - \frac{THE(x+yFR)}{THE(EVA)}\right) \times \frac{y}{(x+y)}\right)} \quad (4)$$

Table 6 presents the results from SE calculations for THE and MARHE, according to equation (3) and equation (4). Equation (3) assumes the superposition of EVA/LW10 and EVA/APP20 or EVA/eAPP20 compared to the combination of both LW and FR-additive in EVA. Equation (4) utilizes the result of P-FR-loadings equal to the total loading (30 wt-%) and adjusts for relative quantities (y/(x + y) = 2/3).

The results presented in Table 6 showcase the synergistic capabilities of LW and FR-additives in EVA composites. All *SE* values with respect of THE are greater than 1, indicating synergy of LW with the P-FRs in EVA; notably, APP exhibited a higher synergy with LW than with eAPP, likely due to the overall good fire performance of eAPP in EVA. For MARHE, the *SE* values were significantly higher with SE values greater than 2 and even greater than 4; this phenomenon is explained by the early t_{ig} of EVA/LW10 compared to other EVA composites, as well as the overall reduction of HRR over time of EVA samples with LW and FR-additives. These results illustrate the capabilities of LW to act as a synergist with P-FRs in EVA to reduce fire loads; the high *SE* indices quantify that LW improved the fire performance of flame retarded EVA composites.

The improvement of fire performance of flame retarded EVA samples by LW was exemplified by the residues after fire testing; Fig. 9 depicts the sample residues after cone calorimeter measurements: Fig. 9a shows that the pure EVA material burned with little residue, while EVA/LW10 in Fig. 9b retained only small amounts of carbonaceous flakes. The residues of FR-containing composites are displayed in Fig. 9c to Fig. 9f, where the samples on the left contain APP and those on the right eAPP. Fig. 9c and Fig. 9d contain 20 wt-% FR, and samples with 30 wt-% FR loadings are shown in Fig. 9e and Fig. 9f. Notably, EVA/eAPP20 and EVA/eAPP30 formed a more carbonaceous residue than EVA/APP20 and EVA/APP30. The EVA-FR composites exhibited a subdued residue formation, which appeared as a mixture of carbonaceous char and inorganic phosphorus residues. These char residues were visibly hygroscopic, they showed increased water uptake several minutes after testing. The EVA samples with LW and APP or eAPP are exhibited in Fig. 9g and Fig. 9h, respectively. These samples are also shown from the side to illustrate the increase in volume in Fig. 9i and Fig. 9j. These images highlight the ability of LW to form carbonaceous residues in combination with phosphorus FRs like APP. The residues of EVA/LW10/APP20 and EVA/LW10/eAPP20 were more voluminous and structurally stable carbonaceous residues than any other EVA composite residue, which had a positive effect on the fire performance of EVA via lower PHRR, THE, and EHC. Increased residue formation was a key mode of action of EVA composites containing both LW and FR. The combination of FR with LW in EVA led to higher residue yields compared to EVA composites containing only FRs at equal loadings. Therefore, LW improved the residue formation of EVA-FR composites; LW acted as a charring agent which interacted with EVA and phosphorus FRs during decomposition, thereby improving the structure and morphology of the char residues.

4.3. Chemical mechanism of flame retardancy in EVA-FR samples with leather waste

Understanding the chemical interactions of EVA, LW, and the P-FRs APP or eAPP in a fire scenario is the key to understanding the macroscopic phenomena observed in fire behavior tests. Scheme 1 displays the decomposition mechanism of EVA as well as flame retarded EVA with APP.

The thermal decomposition of EVA is complex and involves hydrolysis and deacetylation [39]. The first decomposition step occurs at T_1, the main products are acetic acid and acetaldehyde; ethylene–vinyl alcohol is retained. In the second decomposition step at T_{max}, dehydration and depolymerization reactions occur, leading to vaporization of the short chain hydrocarbons. The material decomposes, gasifies, and retains little residue; this behavior was observed in TGA, evolved gas analysis, and cone calorimeter measurements.

In EVA-APP composites, the first decomposition step of EVA overlaps with the decomposition temperature of APP: the materials interact in the condensed phase, leading to phosphorylation and hydrolysis reactions during the deacetylation step of EVA, producing various phosphorylated hydrocarbons. Moreover, the secondary hydroxyls of deacetylated EVA, i.e., ethyl vinyl alcohol,

Table 6
Calculated relative synergistic effect (SE_{rel}), according to equation (3) ($SE_{rel}^{(1)}$) and equation (4) ($SE_{rel}^{(2)}$).

Sample	$SE_{rel}^{(1)}$ (THE)	$SE_{rel}^{(2)}$ (THE)	$SE_{rel}^{(1)}$ (MARHE)	$SE_{rel}^{(2)}$ (MARHE)
EVA/LW10/APP20	1.10 ± 0.10	1.44 ± 0.13	2.58 ± 0.22	4.44 ± 0.38
EVA/LW10/eAPP20	1.04 ± 0.09	1.22 ± 0.11	2.60 ± 0.22	2.71 ± 0.23

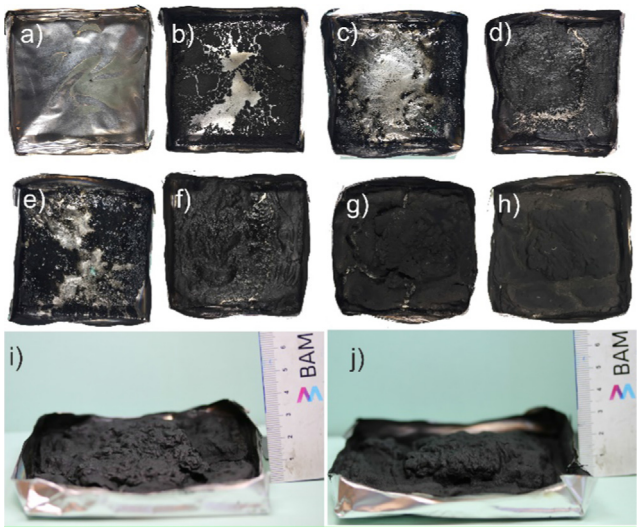

Fig. 9. Residues from cone calorimeter measurements; a) EVA; b) EVA/LW10; c) EVA/APP20; d) EVA/eAPP20; e) EVA/APP30; f) EVA/eAPP30; g) EVA/LW10/APP20; h) EVA/LW10/eAPP20; i) side view of EVA/LW10/APP20; j) side view of EVA/LW10/eAPP20.

may be phosphorylated by APP, which ultimately leads to the formation of some short-chained, phosphorylated hydrocarbons that vaporize. Some polyaromatic P, P-N, P-O, and N-containing residues, as well as hygroscopic polyphosphates and inorganic residues, are retained. The macroscopic phenomenon of charring is the main condensed phase mechanism of APP: the formation of phosphorus-rich aggregates of carbonaceous char increases fuel retention and inhibits burning combustion. The decrease in fire load, the increase in residue, and the decreased effective heat of combustion are evidence of this decomposition pathway.

Scheme 2 exhibits the proposed decomposition mechanism of the EVA-LW composite. The two components EVA and LW decompose at different temperatures, approx. 100 °C apart; thus, only little interaction occurs between them, ultimately leading to decomposition and gasification of the components with only low residue yields. The overlap of decomposition temperature ranges is crucial to the chemical interaction of flame-retardant components [57].

The structure of collagen in LW helps explain the flame-retardant efficacy in FR-containing EVA composites. Generally, the collagen macromolecule contains many polar groups relevant for flame retardant phosphorus chemistry, such as carboxylic acids, amines, hydroxyls, etc. Moreover, tropocollagen molecules contain high concentrations of hydroxyl groups from hydroxyproline, as discussed in Fig. 2. Therefore, the flame retardancy potential of LW is rooted in the chemical structure of collagen and its possible interaction with other decomposition products in flame retarded polymer composites during fires.

The combination of LW and FR in EVA samples had a profound effect on the fire performance. For EVA composites containing both LW and APP or eAPP, the interaction of APP with the EVA grafted with LW via MAH is apparent from the possible phosphorylation targets. Decomposition products of the polymer matrix often con-

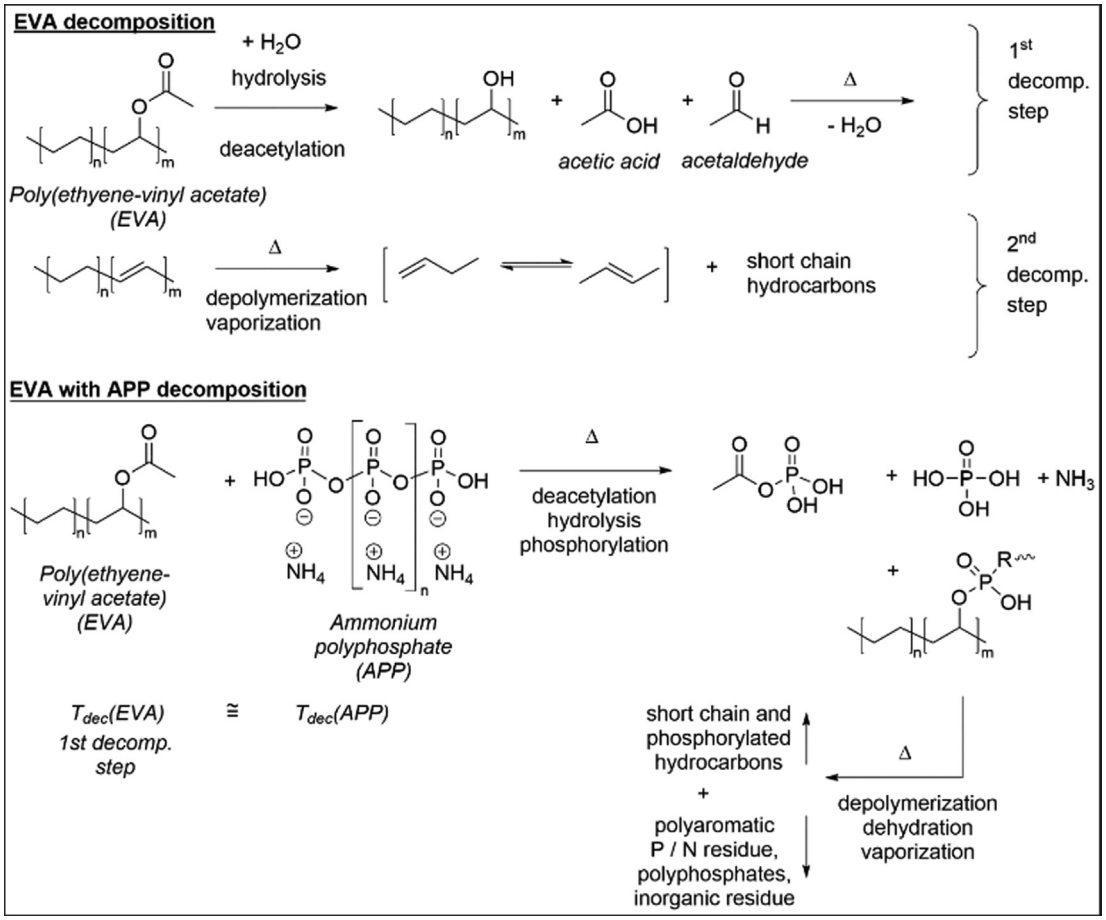

Scheme 1. Proposed decomposition mechanism of EVA, and of EVA when APP is present.

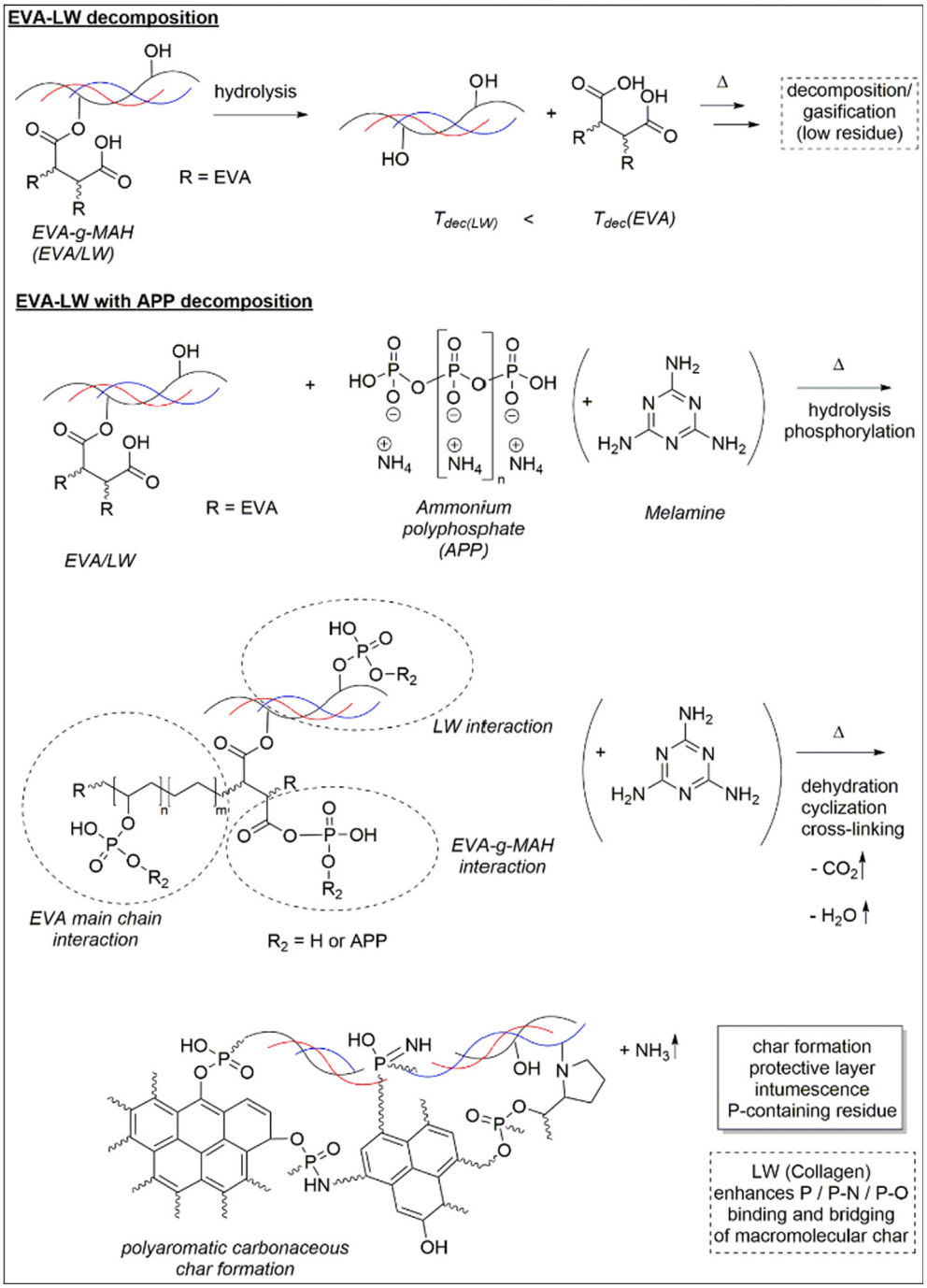

Scheme 2. Proposed decomposition mechanism of EVA composites with APP and LW.

tain polar groups, which are particularly susceptible to phosphorylation during the dynamic, high energy system prevalent in a burning material. These phosphorylated compounds, depending on mass or dimension, are either volatized into the gas phase, or retained in the condensed phase during pyrolysis. Previous studies have shown the various interaction routes between FR and matrix in the condensed phase during decomposition [46]. APP can interact with the many polar groups present in LW, such as hydroxyl groups from hydroxyproline or carboxylic acids. It can interact with carboxylic groups from MAH, or with the deacetylated EVA main chain with secondary hydroxyl groups of ethylene–vinyl alcohol. This abundance of reactive sites increases the presence of phosphorus in all EVA/LW moieties, leading to the vaporization of some P-containing species as well as the retention of P-rich polyaromatic char. P-species act as net-points between the decomposing collagen from LW and the decomposing EVA matrix. This reaction results in increased residue retention, i.e., char formation, where phosphorylation via transesterification occur, while the polymer undergoes dehydration and cyclisation reactions [58,59]. Moreover, the presence of phosphorus and nitrogen compounds in the flame retardant formulation has been shown to produce a more pronounced condensed phase mode of action [60]; the formation of P-N compounds like phosphorus oxynitrides and phosphazenes increases residue formation and stability [42,61]. Additional ammonia released by melamine in eAPP-containing composites acts as a blowing agent, improving intumescence of

the multicellular char [62]; ammonia also acts as a flame dilution agent. The gas phase mode of action of this flame retardant was quantified from reductions in EHC values. The condensed phase mode of action was quantified by increases in residues in pyrolysis and fire testing, as well as the clear intumescent and protective layer effect in cone calorimeter testing. The interaction of LW, FR, and matrix was proven qualitatively by condensed phase FTIR, where the formation of ureas or polyaromatic hydrocarbons were detected. The presented decomposition model serves as a general mechanism to outline the interaction between LW, FR, and EVA based on known flame retardancy mechanisms [63–65]. Further studies into the specific interaction of complex organic compounds like LW with polymers and flame retardants in the condensed phase are on the rise [66–69], and more studies will prove useful to further elucidate the chemical mechanisms at play during decomposition.

5. Conclusions

The investigation of leather waste (LW) from tanneries as a functional filler to flame retarded poly(ethylene–vinyl acetate) (EVA) composites with phosphorus flame retardants (P-FRs) ammonium polyphosphate (APP) or melamine-encapsulated APP (eAPP) yielded interesting results and illuminated the practical use of waste materials from the leather tanning industry as effective fillers to flame retarded polymers.

When 20 wt-% flame retardants (FRs) were added to EVA grafted with 10 wt-% LW via maleic anhydride (samples EVA/LW10/APP20 and EVA/LW10/eAPP20), these composites exhibited reinforced mechanical properties compared to pure EVA, e.g., increased Young's modulus and only slightly lowered tensile strength. They displayed improved flame retardancy behavior compared to 30 wt-% FRs loadings, e.g., lower fire loads, lower peak of heat release rates, and reduced effective heats of combustion. In thermogravimetric pyrolysis experiments and especially in reaction-to-small flames and forced flaming conditions, EVA composites with LW and FRs produced higher residue yields than pure EVA, and yielded more effective intumescent char yields that acted as protective layers than equal (30 wt-%) loadings of only FR.

When LW was grafted to EVA via maleic anhydride (MAH), the polymer-filler mixture reacted more intensely with a P-FR like APP, because additional polar reactive groups (e.g., hydroxyl, carbonyl, etc.) were phosphorylated and cross-linked via various P/P-N/P-O bonds. On the other hand, EVA/LW10 did not exhibit any meaningful flame-retardant behavior, because the matrix and filler decomposed at different temperatures (ΔT = approx. 100 °C). When the FRs APP or eAPP were compounded into EVA grafted with LW, the decomposition temperatures of FR and LW exhibited an overlap in pyrolysis investigations, implying that these materials more easily interacted in the condensed phase during decomposition. This reaction enabled cross-linking reactions between APP, LW, and EVA via the phosphorylation of ethylene–vinyl alcohols formed during the decomposition of the matrix; at elevated temperatures, the composites formed a polyaromatic intumescent char that was able to act via fuel retention and protective layer effects. The melamine present in eAPP acted as a blowing agent, as evidenced by the voluminous char. Thus, the investigation of LW in flame retarded EVA composites illustrated the capabilities of LW to synergize well with P-FRs to lower fire loads.

Utilizing leather wastes from tanneries as effective flame retardant adjuvants in polymer matrices achieves two aims at one: one the one hand, it valorizes the industrial wastes that otherwise require complex waste management solutions, while improving the fire performance of flame retarded polymer matrices on the other hand. Therefore, the results from this investigation further highlight the ability for the fields of polymer science and materials industry to overlap, to achieve the often desired, yet seldom attained goal of creating circular economies with a zero-waste policy. The well-designed valorization, repurposing, or up-cycling of waste products or resources from industries is a pathway towards ultimately reducing the need for costly alternatives in future – waste not, want not.

Funding

This research did not receive any specific grant from funding agencies in the public, commercial, or not-for-profit sectors.

Data availability

Data is available upon request.

CRediT authorship contribution statement

A. Battig: Formal analysis, Investigation, Writing – original draft, Writing – review & editing, Visualization, Project administration. **G. Sanchez-Olivares:** Conceptualization, Formal analysis, Investigation, Resources, Writing – original draft, Writing – review & editing, Visualization, Supervision, Project administration. **D. Rockel:** Investigation, Writing – original draft, Visualization. **M. Maldonado-Santoyo:** Investigation. **B. Schartel:** Conceptualization, Writing – original draft, Writing – review & editing, Supervision, Project administration.

Declaration of Competing Interest

The authors declare that they have no known competing financial interests or personal relationships that could have appeared to influence the work reported in this paper.

Appendix A. Supplementary material

Supplementary data to this article can be found online at https://doi.org/10.1016/j.matdes.2021.110100.

References

[1] A. Schubert, Process control of leather quality, in: F. O'Flaherty, W.T. Roddy, R. M. Lollar (Eds.), The Chemistry and Technology of Leather, Robert E. Krieger Publishing Company, Malabar, FL, USA, 1978, pp. 205–214.
[2] C.V.T. Rigueto, M. Rosseto, D.D.C. Krein, B.E.P. Ostwald, L.A. Massuda, B.B. Zanella, A. Dettmer, Alternative uses for tannery wastes: a review of environmental, sustainability, and science, J. Leather Sci. Eng. 2 (1) (2020) 21, https://doi.org/10.1186/s42825-020-00034-z.
[3] International Council of Tanners, Top 30 world leather producers (million square feet), 2015. https://leathercouncil.org/information/statistics-sources-of-information/. (Accessed 06.05.2021 2021).
[4] Z.N. Azwa, B.F. Yousif, A.C. Manalo, W. Karunasena, A review on the degradability of polymeric composites based on natural fibres, Mater. Des. 47 (2013) 424–442, https://doi.org/10.1016/j.matdes.2012.11.025.
[5] H.M. Akil, M.F. Omar, A.A.M. Mazuki, S. Safiee, Z.A.M. Ishak, A. Abu Bakar, Kenaf fiber reinforced composites: A review, Mater. Des. 32 (8-9) (2011) 4107–4121, https://doi.org/10.1016/j.matdes.2011.04.008.
[6] N.P.G. Suardana, M.S. Ku, J.K. Lim, Effects of diammonium phosphate on the flammability and mechanical properties of bio-composites, Mater. Des. 32 (4) (2011) 1990–1999, https://doi.org/10.1016/j.matdes.2010.11.069.
[7] F. Shukor, A. Hassan, M.S. Islam, M. Mokhtar, M. Hasan, Effect of ammonium polyphosphate on flame retardancy, thermal stability and mechanical properties of alkali treated kenaf fiber filled PLA biocomposites, Mater. Des. 54 (2014) 425–429, https://doi.org/10.1016/j.matdes.2013.07.095.
[8] M.R. Ruiz, E.R. Budemberg, G.P. da Cunha, F.S. Bellucci, H.N. da Cunha, A.E. Job, An innovative material based on natural rubber and leather tannery waste to be applied as antistatic flooring, J. Appl. Polym. Sci. 132 (3) (2015), https://doi.org/10.1002/app.41297.
[9] T. Ambone, S. Joseph, E. Deenadayalan, S. Mishra, S. Jaisankar, P. Saravanan, Polylactic Acid (PLA) Biocomposites Filled with Waste Leather Buff (WLB), J.

Polym. Environ. 25 (4) (2017) 1099–1109, https://doi.org/10.1007/s10924-016-0891-3.
[10] S. Joseph, T.S. Ambone, A.V. Salvekar, S.N. Jaisankar, P. Saravanan, E. Deenadayalan, Processing and characterization of waste leather based polycaprolactone biocomposites, Polym. Compos. 38 (12) (2017) 2889–2897, https://doi.org/10.1002/pc.23891.
[11] B. Ramaraj, Mechanical and thermal properties of ABS and leather waste composites, J. Appl. Polym. Sci. 101 (5) (2006) 3062–3066, https://doi.org/10.1002/app.24113.
[12] Y. Zhang, B. Wang, H. Sheng, B. Yuan, B. Yu, G. Tang, G. Jie, H. Feng, Y. Tao, Y. Hu, Enhanced fire-retardancy of poly(ethylene vinyl acetate) electrical cable coatings containing microencapsulated ammonium polyphosphate as intumescent flame retardant, RSC Adv. 6 (88) (2016) 85564–85573, https://doi.org/10.1039/C6RA15314C.
[13] D.N. Saheb, J.P. Jog, Natural fiber polymer composites: A review, Adv. Polym. Tech. 18 (4) (1999) 351–363, https://doi.org/10.1002/(SICI)1098-2329(199924)18:4<351::AID-ADV6>3.0.CO;2-X.
[14] S. Matkó, A. Toldy, S. Keszei, P. Anna, G. Bertalan, G. Marosi, Flame retardancy of biodegradable polymers and biocomposites, Polym. Degrad. Stab. 88 (1) (2005) 138–145, https://doi.org/10.1016/j.polymdegradstab.2004.02.023.
[15] B.K. Kandola, Flame Retardant Characteristics of Natural Fibre Composites, in: M.J. John, S. Thomas (Eds.) Natural Polymers: Volume 1: Composites, The Royal Society of Chemistry, Cambridge, UK, 2012, Chapter 5, pp. 86–117.
[16] S. Rabe, G. Sanchez-Olivares, R. Pérez-Chávez, B. Schartel, Natural Keratin and Coconut Fibres from Industrial Wastes in Flame Retarded Thermoplastic Starch Biocomposites, Materials 12 (3) (2019) 344, https://doi.org/10.3390/ma12030344.
[17] G. Sanchez-Olivares, S. Rabe, R. Pérez-Chávez, F. Calderas, B. Schartel, Industrial-waste agave fibres in flame-retarded thermoplastic starch biocomposites, Compos. B Eng. 177 (2019) 107370, https://doi.org/10.1016/j.compositesb:2019.107370.
[18] A.D. Covington, Modern tanning chemistry, Chem. Soc. Rev. 26 (2) (1997) 111–126, https://doi.org/10.1039/CS9972600111.
[19] B.M. Haines, J.R. Barlow, The anatomy of leather, J. Mater. Sci. 10 (3) (1975) 525–538, https://doi.org/10.1007/BF00543698.
[20] Nomenclature and Symbolism for Amino Acids and Peptides, Eur. J. Biochem. 138(1) (1984) 9-37. https://doi.org/10.1111/j.1432-1033.1984.tb07877.x.
[21] J.H. Bowes, R.G. Elliott, J.A. Moss, The composition of collagen and acid-soluble collagen of bovine skin, Biochem J 61 (1) (1955) 143–150, https://doi.org/10.1042/bj0610143.
[22] B. Brodsky, A.V. Persikov, Molecular Structure of the Collagen Triple Helix, Advances in Protein Chemistry, Academic Press, 2005, pp. 301–339. https://doi.org/10.1016/S0065-3233(05)70009-7.
[23] V. Ottani, M. Raspanti, A. Ruggeri, Collagen structure and functional implications, Micron 32 (3) (2001) 251–260, https://doi.org/10.1016/s0968-4328(00)00042-1.
[24] N.M. Siviram, D. Barik, Toxic Waste from Leather Industries, in: D. Barik (Ed.), Energy from Toxic Organic Waste for Heat and Power Generation, Elsevier, Duxford, UK, 2019, pp. 55–67.
[25] A.E. Bonilla-Blancas, I.C. Romero-Ibarra, J. Vazquez-Arenas, A. Sanchez-Solis, O. Manero, J. Alvarez-Ramirez, Molecular interactions arising in polyethylene-bentonite nanocomposites, J. Appl. Polym. Sci. 136 (2) (2019) 46920, https://doi.org/10.1002/app.46920.
[26] S.J. Kim, B.S. Shin, J.L. Hong, W.J. Cho, C.S. Ha, Reactive compatibilization of the PBT/EVA blend by maleic anhydride, Polymer 42 (9) (2001) 4073–4080, https://doi.org/10.1016/S0032-3861(00)00810-7.
[27] S.W. Hwang, H.C. Ryu, S.W. Kim, H.Y. Park, K.H. Seo, Grafting maleic anhydride onto EVA and effect on the physical and rheological properties of PETG/EVA-g-MAH blends, J. Appl. Polym. Sci. 125 (4) (2012) 2732–2739, https://doi.org/10.1002/app.36592.
[28] D.G. Dikobe, A.S. Luyt, Morphology and thermal properties of maleic anhydride grafted polypropylene/ethylene–vinyl acetate copolymer/wood powder blend composites, J. Appl. Polym. Sci. 116 (6) (2010) 3193–3201, https://doi.org/10.1002/app.31630.
[29] B. Schartel, M. Bartholmai, U. Knoll, Some comments on the use of cone calorimeter data, Polym. Degrad. Stab. 88 (3) (2005) 540–547, https://doi.org/10.1016/j.polymdegradstab.2004.12.016.
[30] L. Mohammed, M.N.M. Ansari, G. Pua, M. Jawaid, M. Saiful Islam, A Review on Natural Fiber Reinforced Composite and Its Application, Int. J. Polym. Sci. (2015) 243947, https://doi.org/10.1155/2015/243947.
[31] G. Sanchez-Olivares, A. Sanchez-Solis, F. Calderas, L. Medina-Torres, E.E. Herrera-Valencia, J.I. Castro-Aranda, O. Manero, A. Di Blasio, J. Alongi, Flame retardant high density polyethylene optimized by on-line ultrasound extrusion, Polym. Degrad. Stab. 98 (11) (2013) 2153–2160, https://doi.org/10.1016/j.polymdegradstab.2013.09.001.
[32] G. Sanchez-Olivares, A. Sanchez-Solis, O. Manero, R. Pérez-Chávez, M. Jaramillo, J. Alongi, F. Carosio, Improving Mechanical Properties and Reaction to Fire of EVA/LLDPE Blends for Cable Applications with Melamine Triazine and Bentonite Clay, Materials 12 (15) (2019) 2393, https://doi.org/10.3390/ma12152393.
[33] A. Gallos, G. Paës, F. Allais, J. Beaugrand, Lignocellulosic fibers: a critical review of the extrusion process for enhancement of the properties of natural fiber composites, RSC Adv. 7 (55) (2017) 34638–34654, https://doi.org/10.1039/C7RA05240E.
[34] K.-Y. Guo, Q. Wu, M. Mao, H. Chen, G.-D. Zhang, L. Zhao, J.-F. Gao, P. Song, L.-C. Tang, Water-based hybrid coatings toward mechanically flexible, super-hydrophobic and flame-retardant polyurethane foam nanocomposites with high-efficiency and reliable fire alarm response, Compos. B Eng. 193 (2020) 108017, https://doi.org/10.1016/j.compositesb:2020.108017.
[35] A. Riva, M. Zanetti, M. Braglia, G. Camino, L. Falqui, Thermal degradation and rheological behaviour of EVA/montmorillonite nanocomposites, Polym. Degrad. Stab. 77 (2) (2002) 299–304, https://doi.org/10.1016/S0141-3910(02)00065-4.
[36] D.W. van Krevelen, Some basic aspects of flame resistance of polymeric materials, Polymer 16 (8) (1975) 615–620, https://doi.org/10.1016/0032-3861(75)90157-3.
[37] R. Lyon, Plastics and Rubbers, in: C. Harper (Ed.), Handbook of Building Materials for Fire Protection, McGraw-Hill, New York, New York, 2004, pp. 3.1–3.51.
[38] B. Schartel, C.A. Wilkie, G. Camino, Recommendations on the scientific approach to polymer flame retardancy: Part 2—Concepts, J. Fire Sci. 35 (1) (2017) 3–20, https://doi.org/10.1177/0734904116675370.
[39] B.-Å. Sultan, E. Sörvik, Thermal degradation of EVA and EBA—A comparison. I. Volatile decomposition products, J. Appl. Polym. Sci. 43 (9) (1991) 1737–1745, https://doi.org/10.1002/app.1991.070430917.
[40] M. Hesse, H. Meier, B. Zeeh, Spektroskopische Methoden in der organischen Chemie, Georg Thieme Verlag, 2005.
[41] G. Socrates, Infrared and Raman Characteristic Group Frequencies: Tables and Charts, John Wiley & Sons, West Sussex, UK, 2004.
[42] A. Battig, J.C. Markwart, F.R. Wurm, B. Schartel, Hyperbranched phosphorus flame retardants: multifunctional additives for epoxy resins, Polym. Chem. 10 (31) (2019) 4346–4358, https://doi.org/10.1039/C9PY00737G.
[43] L.C. Thomas, Interpretation of the Infrared Spectra of Organophosphorus Compounds, Heyden, London, 1974.
[44] S. Rabe, Y. Chuenban, B. Schartel, Exploring the modes of action of phosphorus-based flame retardants in polymeric systems, Materials 10 (5) (2017) 23, https://doi.org/10.3390/ma10050455.
[45] E. GZallo, G. Sanchez-Olivares, B. Schartel, Flame retardancy of starch-based biocomposites - aluminum hydroxide-coconut fiber synergy, Polimery 58 (5) (2013) 395–402.
[46] B. Schartel, B. Perret, B. Dittrich, M. Ciesielski, J. Krämer, P. Müller, V. Altstädt, L. Zang, M. Döring, Flame Retardancy of Polymers: The Role of Specific Reactions in the Condensed Phase, Macromol. Mater. Eng. 301 (1) (2016) 9–35, https://doi.org/10.1002/mame.201500250.
[47] B. Schartel, K. Kebelmann, Fire Testing for the Development of Flame Retardant Polymeric Materials, in: Y. Hu, X. Wang (Eds.), Flame Retardant Polymeric Materials, CRC Press-Taylor & Francis Group, Boca Raton, 2020.
[48] V. Babrauskas, The Cone Calorimeter, in: M.J. Hurley, D. Gottuk, J.R. Hall Jr., K. Harada, E. Kuligowski, M. Puchovsky, J. Torero, J. M. Watts Jr., C. Wieczorek (Eds.) SFPE Handbook of Fire Protection Engineering, Springer, New York, NY, 2016, Chapter 27, pp. 952–980.
[49] J. Alongi, M. Poskovic, A. Frache, F. Trotta, Novel flame retardants containing cyclodextrin nanosponges and phosphorus compounds to enhance EVA combustion properties, Polym. Degrad. Stab. 95 (10) (2010) 2093–2100, https://doi.org/10.1016/j.polymdegradstab.2010.06.030.
[50] R. Petrella, The assessment of full-scale fire hazards from cone calorimeter data, J. Fire Sci. 12 (1) (1994) 14–43, https://doi.org/10.1177/073490419401200102.
[51] H. Vahabi, B.K. Kandola, M.R. Saeb, Flame Retardancy Index for Thermoplastic Composites, Polymers 11 (3) (2019) 407, https://doi.org/10.3390/polym11030407.
[52] K. Langfeld, A. Wilke, A. Sut, S. Greiser, B. Ulmer, V. Andrievici, P. Limbach, M. Bastian, B. Schartel, Halogen-free fire retardant styrene-ethylene-butylene-styrene-based thermoplastic elastomers using synergistic aluminum diethylphosphinate-based combinations, J. Fire Sci. 33 (2) (2015) 157–177, https://doi.org/10.1177/0734904114565581.
[53] M.-C. Despinasse, B. Schartel, Aryl phosphate–aryl phosphate synergy in flame-retarded bisphenol A polycarbonate/acrylonitrile-butadiene-styrene, Thermochim Acta 563 (2013) 51–61, https://doi.org/10.1016/j.tca.2013.04.006.
[54] E.D. Weil, Synergists, Adjuvants, and Antagonists in Flame-Retardant Systems, in: A.F. Grand, C.A. Wilkie (Eds.), Fire Retardancy of Polymeric Materials, Marcel Dekker, New York, NY, 2000, pp. 115–145.
[55] M. Lewin, Synergism and catalysis in flame retardancy of polymers, Polym. Adv. Technol. 12 (3-4) (2001) 215–222, https://doi.org/10.1002/pat.v12:3/410.1002/pat.132.
[56] G.M. Wu, B. Schartel, H. Bahr, M. Kleemeier, D. Yu, A. Hartwig, Experimental and quantitative assessment of flame retardancy by the shielding effect in layered silicate epoxy nanocomposites, Combust. Flame 159 (12) (2012) 3616–3623, https://doi.org/10.1016/j.combustflame.2012.07.003.
[57] A. Battig, J.C. Markwart, F.R. Wurm, B. Schartel, Matrix matters: Hyperbranched flame retardants in aliphatic and aromatic epoxy resins, Polym. Degrad. Stab. 170 (2019) 108986, https://doi.org/10.1016/j.polymdegradstab.2019.108986.
[58] S.V. Levchik, Introduction to Flame Retardancy and Polymer Flammability, in: A.B. Morgan, C.A. Wilkie (Eds.), Flame Retardant Polymer Nanocomposites, John Wiley & Sons Inc, Hoboken, NJ, 2007.
[59] J.W. Lyons, Mechanisms of fire retardation with phosphorus compounds: Some speculation, J. Fire Flammability 1 (1970) 302–311.
[60] C. Nguyen, J. Kim, Thermal stabilities and flame retardancies of nitrogen-phopshorus flame retardants based on bisphorphoramidates, Polym. Degrad.

Stab. 93 (6) (2018) 1037–1043, https://doi.org/10.1016/j.polymdegradstab.2008.03.024.
[61] S.V. Levchik, G.F. Levchik, A.I. Balabanovich, E.D. Weil, M. Klatt, Phosphorus oxynitride: a thermally stable fire retardant additive for polyamide 6 and poly (butylene terephthalate), Angew. Makromol. Chem. 264 (1) (1999) 48–55, https://doi.org/10.1002/(SICI)1522-9505(19990201)264:1<48::AID-APMC48>3.0.CO;2-W.
[62] J. Alongi, Z. Han, S. Bourbigot, Intumescence: Tradition versus novelty. A comprehensive review, Progress Polym. Sci. 51 (2015) 28–73, https://doi.org/10.1016/j.progpolymsci.2015.04.010.
[63] J. Green, Mechanisms for Flame Retardancy and Smoke suppression – A Review, J. Fire Sci. 14 (6) (1996) 426–442.
[64] J.W. Hastie, Molecular basis of flame inhibition, Journal of Research of the National Bureau of Standards – A, Phys. Chem. 77A (6) (1973) 733–754, https://doi.org/10.6028/jres.077A.045.
[65] J.K. Fink, Mechanisms of Flame Retardants, in: Flame Retardants, Scrivener Publishing, Beverly, MA, 2020, Chapter 2, pp. 131–145.
[66] D.A. Villamil Watson, D.A. Schiraldi, Biomolecules as Flame Retardant Additives for Polymers: A Review, Polymers 12 (4) (2020) 849, https://doi.org/10.3390/polym12040849.
[67] C.E. Hobbs, Recent Advances in Bio-based Flame Retardant Additives for Synthetic Polymer Materials, Polymers 11 (2019) 224, https://doi.org/10.3390/polym11020224.
[68] Y.-Y. Gao, C. Deng, Y.-Y. Du, S.-C. Huang, Y.-Z. Wang, A novel Bio-based Flame Retardant for Polypropylene from Phytic Acid, Polym. Degrad. Stab. 161 (2019) 298–308, https://doi.org/10.1016/j.polymdegradstab.2019.02.005.
[69] L. Passauer, Thermal Characterization of Ammonium Starch Phosphate Carbamates for Potential Applications as Bio-based Flame Retardants, Carbohydr. Polym. 221 (2019) 69–74, https://doi.org/10.1016/j.carbpol.2019.01.100.